Contents lists available at ScienceDirect

Chemical Engineering Research and Design

journal homepage: www.elsevier.com/locate/cherd

The Maxwell–Stefan description of mixture permeation across nanoporous graphene membranes

Rajamani Krishna

Van 't Hoff Institute for Molecular Sciences, University of Amsterdam, Science Park 904, 1098 XH Amsterdam, The Netherlands

ARTICLE INFO

Article history:
Received 7 January 2018
Received in revised form 15 March 2018
Accepted 21 March 2018
Available online 30 March 2018

Keywords:
Surface adsorption
Maxwell–Stefan diffusion
Quasi-chemical theory
Slowing-down effects
Kinetic Monte Carlo simulations

ABSTRACT

There is increasing research interest on the use of two-dimensional (2D) nanoporous materials, such as graphenes and graphene oxides, in a variety of membrane separation applications. The membrane permeation selectivitites are governed by a variety of factors that include surface diffusion as an important constituent. The primary objective of this article is to present a Maxwell–Stefan (M–S) formulation for surface diffusion of binary (1, 2) mixtures on 2D nanoporous graphene surfaces. In the developed formulation, adsorbate–adsorbate interactions, either attractive or repulsive, are described by the quasi-chemical (QC) mean field approximation of Guggenheim. Such interactions have a direct influence on the occupancy dependencies of the M–S diffusivities, $Đ_1$ and $Đ_2$, that quantify molecule-surface "friction". An essential feature of the M–S formulation is the inclusion of exchange coefficients, $Đ_{12}$, that quantify *correlation*, or *slowing-down* effects for surface diffusion; the tardier-more-strongly-adsorbed species usually "slows down" the more-mobile-less-strongly-adsorbed species. Kinetic Monte Carlo (KMC) simulations on 2D square lattice of adsorption sites are used to quantify the the loading dependence of the M–S diffusivities, and also correlation effects. The usefulness of the developed model, combining QC and M–S approaches, is illustrated for CO_2/CH_4, CO_2/H_2, CO_2/N_2, and CH_4/H_2, mixture separations. For all four mixtures, the neglect of correlation effects leads to a severe underestimation of the membrane permeation selectivities that favor the more strongly adsorbed species.

1. Introduction

Two-dimensional (2D) nanoporous materials such as graphenes and graphene oxides, have attracted a lot of interest in recent years for separation of a variety of mixtures of light gases (H_2/CO_2, H_2/N_2, H_2/CH_4, CO_2/N_2, CO_2/CH_4), water/alcohol mixtures, and water purification (Celebi et al., 2014; Gadipelli and Guo, 2015; Kim et al., 2013; Koenig et al., 2012; Li et al., 2013; Liu et al., 2015; Nair et al., 2012; Wang et al., 2017a, 2014). Experimental investigations, on their own, do not provide sufficient insights into the precise mechanisms underlying, and driving, separation selectivities. For this reason, a number of theoretical investigations, largely based on Density Functional Theory (DFT), and Molecular Dynamics (MD) simulations, serve to elucidate the constituent mechanisms contributing to separations (Blankenburg et al., 2010; Du et al., 2011; Hauser and Schwerdtfeger, 2012; Jiao and Xu, 2015; Khakpay et al., 2017; Pedrielli et al., 2017; Schrier, 2012; Solvik et al., 2013; Sun and Bai, 2017a, 2017b; Sun et al., 2014; Wang et al., 2017b; Wen et al., 2015; Yuan et al., 2017). Two different pathways for transmembrane transport of gaseous guest molecules may be identified; see schematic in Fig. 1: (1) fluid-phase pathway that is of prime importance in size-selective separations using graphene layers with pores smaller than say 1 nm (Drahushuk and Strano, 2012), and (2) adsorbed-phase pathway that includes surface adsorption, surface diffusion, and pore translocation (Drahushuk and Strano, 2012; Jiao and Xu, 2015; Sun and

E-mail address: r.krishna@contact.uva.nl
https://doi.org/10.1016/j.cherd.2018.03.033

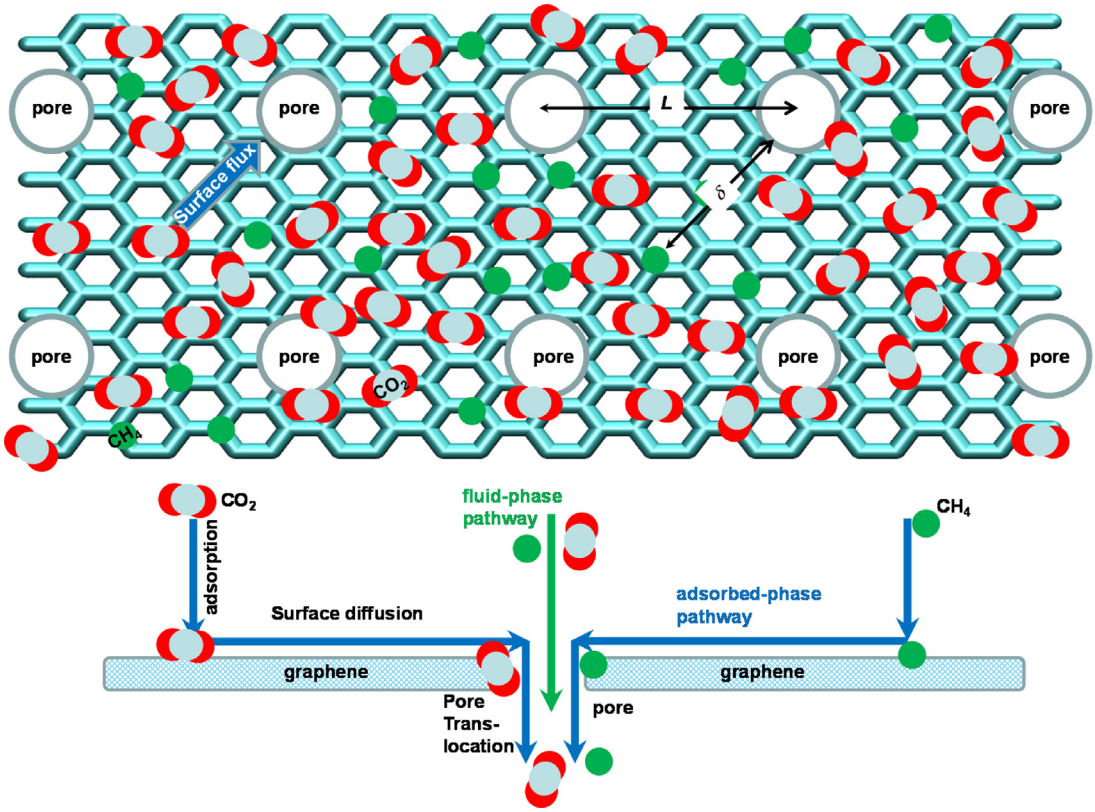

Fig. 1 – Schematic showing transport mechanisms across 2D graphene membrane. Implicit in this schematic is that the inter-pore spacing is significantly larger than the length scale characteristics of surface diffusion; see Drahushuk and Strano (2012).

Bai, 2017a; Sun et al., 2014; Yuan et al., 2017). For gaseous mixtures, the flux contribution of the gas-phase pathway, also termed the "direct flux" (Sun and Bai, 2017a, 2017b; Sun et al., 2014), may be calculated using the Knudsen prescription (Celebi et al., 2014; Drahushuk and Strano, 2012; Knudsen, 1909).

The importance of the contribution of the surface flux to the overall permeation flux has been underscored in a number of publications (Du et al., 2011; Schrier, 2012; Shan et al., 2012; Sun and Bai, 2017a; Sun et al., 2014; Wen et al., 2015). For permeation of guest species such as CO_2, and CH_4, that adsorb strongly on the surface, the contribution of the surface diffusion flux may often be significant fraction of the overall permeation flux (Schrier, 2012; Sun and Bai, 2017a; Sun et al., 2014). For H_2/N_2 separations, Du et al. (2011) demonstrate that the separations are H_2-selective for smaller pore sizes, whereas with larger pore sizes, the separations become N_2-selective, because of the increasing significance of the contribution of the adsorbed-phase pathway. Shan et al. (2012) demonstrate the possibility of increasing the CO_2/N_2 selectivities in porous graphene membranes by chemical functionalization of the graphene sheet and the pore rim, thereby enhancing the adsorption strength of CO_2. For CH_4/H_2 and CH_4/N_2 separations, the more strongly adsorbed CH_4 has the effect of reducing the permeance of partner species, H_2 and N_2; this effect is termed "inhibition" by Wen et al. (2015). Solvik et al. (2013) demonstrate how entropy effects in adsorption may be exploited for separations of ethene/ethane, propene/propane, *n*-butane/1,3-butadiene, and butene isomer mixtures.

Generally speaking, the relative importance of the different transport mechanisms, sketched in Fig. 1, depends on a variety of factors that include pore size, pore geometry and shape, spacing between pores, adsorption strength on surface and pore rim, and surface mobilities of the adsorbates (Drahushuk and Strano, 2012; Jiao and Xu, 2015; Sun and Bai, 2017a; Sun et al., 2014; Yuan et al., 2017). This article provides a quantitative analysis of the scenario in which the adsorbed-phase pathway is the main determinant of membrane permeation rates and selectivities. The primary objective is to develop a model for mixture diffusion of adsorbates along the 2D graphene surface in the direction of the pores, a precursor to pore translocation. We aim to explore, and elucidate, the subtle interplay between relative adsorption strengths and mobilities, that influence the permeation selectivities. The "inhibition" effect exerted by the more strongly adsorbed species, as highlighted by Wen et al. (2015), is shown to have two distinct origins: (1) competitive mixture adsorption, and (2) *correlation* effects in surface diffusion of mixtures. To meet the objectives set above, we adopt the Maxwell–Stefan (M–S) formalism to describe the 2D surface diffusion fluxes (Krishna, 1990, 2009, 2017). For quantifying the correlation effects that are of prime importance in surface diffusion, we resort to Kinetic Monte Carlo (KMC) simulations using the methodology described in published works (Krishna et al., 2004; Paschek and Krishna, 2000, 2001a, 2001b).

2. The Maxwell–Stefan description of mixture diffusion on 2D surfaces

The M–S equations represent a balance between the force exerted per mole of species *i* with the drag, or friction, experienced with each of the partner species in the mixture (Krishna, 2015, 2016a). We may expect that the frictional drag to be proportional to differences in the velocities of the diffusing species $(u_i - u_j)$, where u_i is the velocity of motion of the adsorbate on the 2D surface, that is considered to be stationary. For a mixture containing a total of *n* penetrants, the M–S equations take the form (Krishna, 2017)

$$-\frac{d\mu_i}{dz} = \sum_{j=1;j\neq i}^{n} \frac{RT}{Đ_{ij}} x_j (u_j - u_n) + \frac{RT}{Đ_i}(u_i); \quad i = 1, 2, .. n \tag{1}$$

The left members of Eq. (1) are the negative of the gradients of the chemical potentials, with the units $N\,mol^{-1}$; it represents the driving force acting per mole of species *i*. We define

Notation

b_i	Parameter in the pure component Langmuir adsorption isotherm, Pa^{-1}
[B]	Matrix of inverse Maxwell–Stefan coefficients, $m^{-2}\,s$
d_{pore}	Pore diameter, m
$Đ_i$	M–S diffusivity of component i for molecule-surface interactions, $m^2\,s^{-1}$
$Đ_i(0)$	M–S diffusivity at zero-loading, $m^2\,s^{-1}$
$Đ_{ij}$	M–S exchange coefficient, $m^2\,s^{-1}$
$Đ_{12}$	M–S exchange coefficient for binary mixture, $m^2\,s^{-1}$
$D_{i,self}$	Self-diffusivity of species i, $m^2\,s^{-1}$
f_i	Partial fugacity of species i, Pa
L	Inter-pore spacing on graphene layer, m
n	Number of penetrants, dimensionless
N_i	Molar flux of species i, $mol\,m^{-2}\,s^{-1}$
p_i	Partial pressure of species i, Pa
p_t	Total system pressure, Pa
q_i	Molar loading of species i, $mol\,kg^{-1}$
$q_{i,sat}$	Molar loading of species i at saturation, $mol\,kg^{-1}$
q_t	Total molar loading of mixture, $mol\,kg^{-1}$
$\mathbf{r}_{l,i}(t)$	Position vector for molecule l of species i at any time t, m
R	Gas constant, $8.314\,J\,mol^{-1}\,K^{-1}$
T	Absolute temperature, K
u_i	Velocity of motion of i, $m\,s^{-1}$
w	Energy of interaction, $J\,mol^{-1}$
x_i	Mole fraction of species i in adsorbed phase, dimensionless
z	Distance coordinate, m

Greek letters

β	Parameter defined in Eq. (9), dimensionless
Γ_{ij}	Thermodynamic factors, dimensionless
[Γ]	Matrix of thermodynamic factors, dimensionless
δ	Diffusion distance as indicated in Fig. 1, m
ε	Fractional pore area relative to membrane area, dimensionless
ζ	Coordination number, dimensionless
η	Dimensionless distance, dimensionless
θ_i	Fractional occupancy of component i, dimensionless
θ_t	Fractional occupancy of adsorbed mixture, dimensionless
λ	Jump distance on 2D lattice, m
[Λ]	Matrix of Maxwell–Stefan diffusivities, $m^2\,s^{-1}$
μ_i	Molar chemical potential, $J\,mol^{-1}$
ν	Jump frequency, s^{-1}
ϕ	Parameter defined in Eq. (9), dimensionless
ρ	Mass density of graphene layer, $kg\,m^{-3}$

Subscripts

1	Referring to species 1
2	Referring to species 2
i,j	Components in mixture
i	Referring to component i
t	Referring to total mixture
sat	Referring to saturation conditions

Vector and matrix notation

()	Component vector
[]	Square matrix

the mole fractions of the components in the adsorbed phase, x_i:

$$x_i = q_i/q_t \tag{2}$$

where q_i is the molar loading of adsorbate i, expressed say as moles per kg of graphene, and q_t is the total mixture loading $q_t = \sum_{i=1}^{n} q_i$.

The term $RT/Đ_i$ is interpreted as the drag or friction coefficient between the penetrant i and the membrane. The term $RT/Đ_{ij}$ is interpreted as the friction coefficient for the $i-j$ pair of penetrants. At the molecular level, the coefficients $Đ_{ij}$ reflect how the facility for transport of species i *correlates* with that of species j; they are also termed *exchange coefficients*. The inclusion of such correlation effects is vital because the tardier-more-strongly-adsorbed species usually "slows down" the more-mobile-less-strongly-adsorbed species, as shall be demonstrated later in this article.

The Maxwell–Stefan diffusion formulation (1) is consistent with the theory of irreversible thermodynamics; the Onsager Reciprocal Relations imply that the M–S pair diffusivities are symmetric

$$Đ_{ij} = Đ_{ji} \tag{3}$$

For uniformly spaced pores, each say of diameter d_{pore}, with inter-pore spacing L, the maximum distance to be traversed along the surface for any adsorbate is $\delta = \frac{\sqrt{2}L - d_{pore}}{2}$. The area fraction of pores relative to the total membrane cross-sectional area is $\varepsilon = \frac{\pi d_{pore}^2/4}{L^2}$; the fractional area available for surface adsorption is $1-\varepsilon$. The membrane permeation flux, defined as the number of moles transported across the membrane per second per m^2 of total membrane surface area is

$$N_i \equiv (1-\varepsilon)\,\rho q_i u_i \tag{4}$$

In Eq. (4), ρ is the mass density of the graphene layer, expressed in the units of $kg\,m^{-3}$. Multiplying both sides of Eq. (1) by $(1-\varepsilon)\,q_i$, the M–S equations take the form (Krishna, 2014, 2016b, 2017; Krishna and van Baten, 2011)

$$-\rho(1-\varepsilon)\frac{q_i}{RT}\frac{d\mu_i}{dz} = \sum_{\substack{j=1\\ j\neq i}}^{n} \frac{x_j N_i - x_i N_j}{Đ_{ij}} + \frac{N_i}{Đ_i}; \quad i = 1, 2, ..n \tag{5}$$

The chemical potential of component i in the adsorbed phase equals the chemical potential of that component in the bulk fluid mixture, i.e. $d\mu_i = RTd\ln f_i$, where f_i is the partial fugacity in the bulk fluid phase. The chemical potential gradients $d\mu_i/dz$ can be related to the gradients of the molar loadings, q_i, by defining thermodynamic correction factors Γ_{ij}

$$\frac{q_i}{RT}\frac{d\mu_i}{dz} = \sum_{j=1}^{n}\Gamma_{ij}\frac{dq_j}{dz}; \quad \Gamma_{ij} = \frac{q_i}{f_i}\frac{\partial f_i}{\partial q_j}; \quad i,j = 1, ...n \tag{6}$$

The thermodynamic correction factors Γ_{ij} can be calculated by differentiation of the model describing mixture adsorption equilibrium, that relates the molar loadings, q_i, to the partial fugacities in the bulk fluid mixture, f_i. Generally speaking, the Ideal Adsorbed Solution Theory (IAST) of Myers and Prausnitz (1965) is the preferred method for estimation of mixture adsorption equilibrium.

Though a limited number of MD simulation data on *unary* self-diffusivities have been reported (Jiao and Xu, 2015; Sun and Bai, 2017a, 2017b; Sun et al., 2014), to our knowledge, there is no available MD or experimental data on the M–S diffusivities $Đ_i$, and $Đ_{ij}$ that are required in the use of Eq. (5) to calculate surface diffusion fluxes. The subsequent sections of this article address the following set of questions.

(1) How do the M–S diffusivities $Đ_i$ depend on the molar loadings, q_i?
(2) Are the coefficients $Đ_i$ characterizing unary diffusion identifiable with those describing mixture diffusion?
(3) How do adsorbate–adsorbate interactions influence the $Đ_i$?
(4) How do we estimate the exchange coefficients $Đ_{ij}$?
(5) How do the exchange coefficients $Đ_{ij}$ influence the membrane separation selectivities?

3. Unary diffusion on a square array of adsorption sites

The 2D surface may be viewed as consisting of a square array of adsorption sites. A molecule, say species i, may hop from one site to an adjacent one, provided that site is vacant. In the simplest scenario, when there are no molecule-molecule interactions, either attractive or repulsive, the jump frequency ν_i is proportional to the fractional vacancy: $\nu_i = \nu_i(0)(1-\theta)$ where $\theta_i = q_i/q_{i,sat}$ is the fractional occupancy. In this scenario, the M–S diffusivity is a linearly decreasing function of occupancy

$$Đ_i = Đ_i(0)(1-\theta_i) \tag{7}$$

In Eq. (7), the M–S diffusivity in the limit of vanishingly small occupancies is $Đ_i(0) = \frac{1}{\zeta}\nu_i(0)\lambda^2$, where ζ is the coordination number of the lattice and λ is the jump distance on the square lattice; for a square lattice, $\zeta = 4$.

More generally, molecule-molecule interactions serve to influence the jump frequencies by a factor that depends on the energy of interaction, w. For repulsive interactions, $w > 0$, whereas for attractive interactions, $w < 0$. Using the quasi-chemical approach of Reed and Ehrlich (1981) to quantify such interactions, the following expression is obtained for the loading dependence of the M–S diffusivities (Krishna et al., 2004; Krishna and van Baten, 2009b)

$$Đ_i = Đ_i(0)\left(\frac{1+\beta_i}{2(1-\theta_i)}\right)^{-\zeta}\left(1+\frac{(\beta_i-1+2\theta_i)\phi}{2(1-\theta_i)}\right)^{\zeta-1} \tag{8}$$

In Eq. (8) the following dimensionless parameters are defined

$$\beta_i = \sqrt{1-4\theta_i(1-\theta_i)(1-1/\phi)}; \quad \phi = \exp(w/RT) \tag{9}$$

In the limiting case of no interactions, $w = 0$, $\phi = 1$, $\beta_i = 1$ and Eq. (7) is recovered. The continuous solid lines in Fig. 2a are the calculations of the occupancy dependence of the normalized

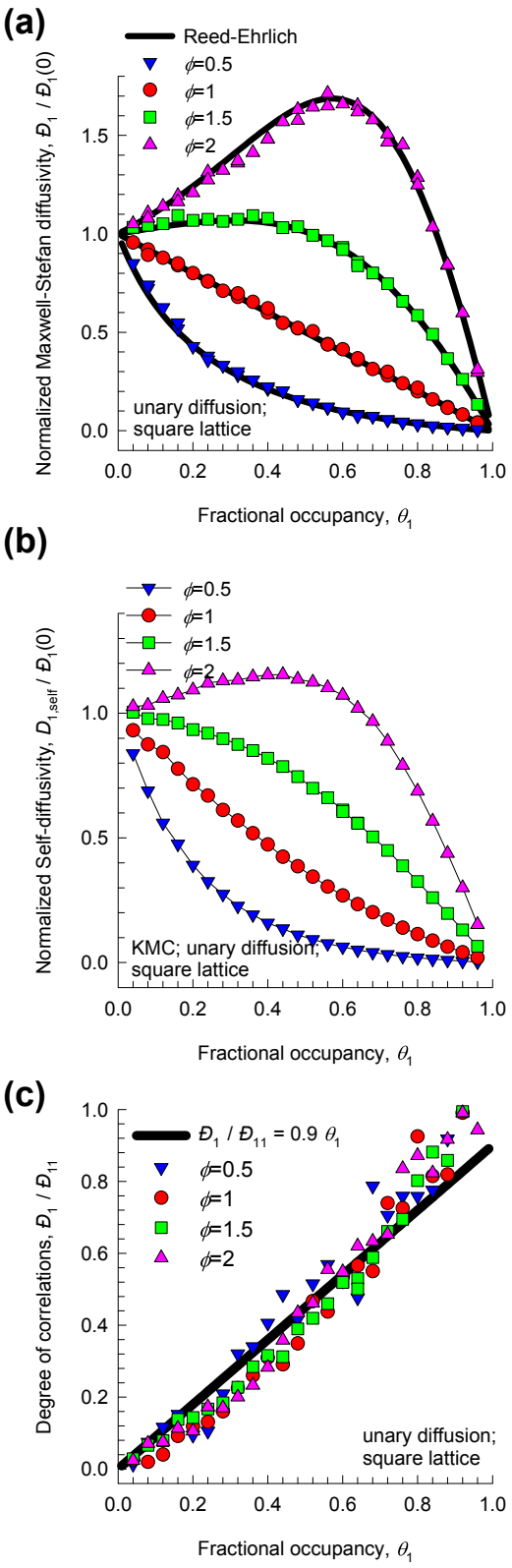

Fig. 2 – KMC simulations (symbols) of normalized (a) Maxwell–Stefan and (b) self-diffusivities on a square lattice, plotted as a function of the fractional occupancy for four different values of $\phi = \exp(w/RT) = 0$, 0.5, 1.5, 2. The continuous solid lines are the calculations using Eqs. (8) and (9). (c) The degree of correlations $Đ_1/Đ_{11}$ plotted as a function of the fractional occupancy.

M–S diffusivity using Eqs. (8), and (9) for four different values of $\phi = \exp(w/RT) = 0, 0.5, 1.5, 2$. The symbols in Fig. 2a are Kinetic Monte Carlo (KMC) simulation data for the M–S diffusivity, $Đ_i$, determined by monitoring the mean square displacement of an *ensemble* of molecules on a square lattice using the methodology described in detailed in our previous works (Krishna et al., 2004; Paschek and Krishna, 2000, 2001a, 2001b). There is excellent match between the KMC simulation data and the Reed–Ehrlich model calculations. In our previous work using MD simulations, we had established the applicability of the Reed–Ehrlich model for diffusion of linear alkanes in carbon nanotubes (Krishna and van Baten, 2006).

The symbols in Fig. 2b are the KMC simulation data for the self-diffusivities, $D_{i,self}$, determined by analyzing the mean square displacement of *individual* molecules. The self-diffusivities are generally lower than the corresponding values of the M–S diffusivities, i.e. $D_{i,self} < Đ_i$; the extent of lowering is due to *correlation* effects; a molecule may jump to a site whence it originated. In order to derive the relation between the self-diffusivities and the M–S diffusivities, we apply Eq. (5) for a binary mixture consisting of tagged, or tracer, species (i*) and untagged species *i* that are otherwise identical; this yields

$$\frac{1}{D_{i,self}} = \frac{1}{Đ_i} + \frac{1}{Đ_{ii}} \tag{10}$$

We define the degree of correlations as

$$\frac{Đ_i}{Đ_{ii}} = \frac{Đ_i}{D_{i,self}} - 1 \tag{11}$$

The degree of correlations determined using Eq. (11) are plotted in Fig. 2c as a function of the fractional occupancy; the dependence is nearly linear. It is interesting to note that correlation effects are practically uninfluenced by the interaction energies, and almost the entire data set lies within the narrow range; the value $\frac{Đ_i}{Đ_{ii}} = 0.9\theta_i$ is a fairly good representation of the entire data set.

For predicting the loading dependence of the M–S diffusivities, we need good estimates of the interaction energies, w_i. In principle, this information can be extracted from the unary adsorption isotherms. Application of the quasi-chemical (QC) mean field approximation of Guggenheim for adsorption on a lattice (Krishna and van Baten, 2013b) yields the relation between the fugacity, f_i, in the gas phase and the fractional occupancy on the surface

$$b_i f_i = \frac{\theta_i}{(1-\theta_i)}\left(\frac{2(1-\theta_i)}{\beta_i + 1 - 2\theta_i}\right)^{\zeta} \tag{12}$$

In the limiting case of no interactions, $w = 0$, $\phi = 1$, $\beta_i = 1$, and Eq. (12) reduces to the Langmuir isotherm $b_i f_i = \frac{\theta_i}{(1-\theta_i)}$, where b_i is the Langmuir adsorption constant. By fitting experimental isotherm data to Eq. (12), we can determine $\phi = \exp(w/RT)$; see illustrative examples in Figs. S5–S7 of the Supplementary material accompanying this publication.

4. Surface diffusion of binary mixtures

For surface diffusion of binary mixtures, the Maxwell–Stefan Eq. (5) reduce to the set of two equations

$$\begin{aligned} -\rho(1-\varepsilon)\frac{q_1}{RT}\frac{d\mu_1}{dz} &= \frac{x_2 N_1 - x_1 N_2}{Đ_{12}} + \frac{N_1}{Đ_1} \\ -\rho(1-\varepsilon)\frac{q_2}{RT}\frac{d\mu_2}{\partial z} &= \frac{x_1 N_2 - x_2 N_1}{Đ_{12}} + \frac{N_2}{Đ_2} \end{aligned} \tag{13}$$

The first members on the right hand side of Eq. (13) are required to quantify slowing-down effects that characterize binary mixture diffusion (Krishna, 2009, 2012; Krishna and van Baten, 2013a). For a binary mixture, the exchange coefficient $Đ_{12}$ can be estimated

by interpolating between the self-exchange coefficients of pure components: $Đ_{11}$ and $Đ_{22}$. On the basis of extensive MD data on mixture diffusivities in zeolites and MOFs the following interpolation formula, based on the Vignes (1966) model for diffusion in liquid mixtures has been proposed (Krishna, 2009, 2012; Krishna and van Baten, 2009a)

$$Đ_{12} = (Đ_{11})^{x_1}(Đ_{22})^{x_2} \tag{14}$$

For surface diffusion on square lattices, the self-exchange coefficients are calculated on the basis of the information presented in Fig. 2c, but based on the total occupancy, $\theta_t = \theta_1 + \theta_2$ $\frac{Đ_i}{Đ_{ii}} = 0.9\theta_t$, and not the individual component occupancies.

Let us define the square matrix [B]

$$[B] = \begin{bmatrix} \frac{1}{Đ_1} + \frac{x_2}{Đ_{12}} & -\frac{x_1}{Đ_{12}} \\ -\frac{x_2}{Đ_{12}} & \frac{1}{Đ_2} + \frac{x_1}{Đ_{12}} \end{bmatrix} \tag{15}$$

Eq. (13) can be re-cast into 2-dimensional matrix notation

$$\begin{aligned} -\rho(1-\varepsilon)\begin{pmatrix} \frac{q_1}{RT}\frac{d\mu_1}{dz} \\ \frac{q_2}{RT}\frac{d\mu_2}{dz} \end{pmatrix} &= [B]\begin{pmatrix} N_1 \\ N_2 \end{pmatrix}; \\ \begin{pmatrix} N_1 \\ N_2 \end{pmatrix} &= -(1-\varepsilon)[B]^{-1}\begin{pmatrix} \frac{q_1}{RT}\frac{d\mu_1}{dz} \\ \frac{q_2}{RT}\frac{d\mu_2}{dz} \end{pmatrix} \end{aligned} \tag{16}$$

We define the square matrix $[\Lambda] \equiv [B]^{-1}$; The inverse of the square matrix [B] can be determined explicitly

$$[\Lambda] \equiv [B]^{-1} = \frac{1}{1 + \frac{x_1 Đ_2}{Đ_{12}} + \frac{x_2 Đ_1}{Đ_{12}}} \begin{bmatrix} Đ_1\left(1 + \frac{x_1 Đ_2}{Đ_{12}}\right) & \frac{x_1 Đ_1 Đ_2}{Đ_{12}} \\ \frac{x_2 Đ_1 Đ_2}{Đ_{12}} & Đ_2\left(1 + \frac{x_2 Đ_1}{Đ_{12}}\right) \end{bmatrix} \tag{17}$$

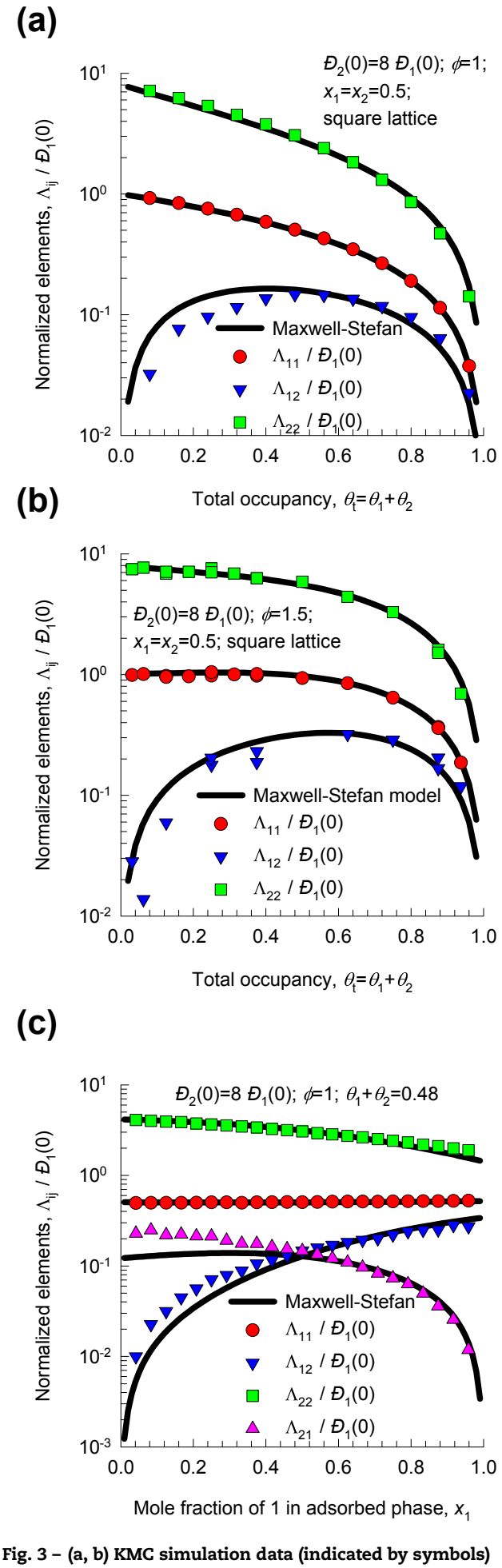

Fig. 3 – (a, b) KMC simulation data (indicated by symbols) for the elements of the Λ_{ij} for equimolar binary mixtures ($x_1 = x_2 = 0.5$), plotted as a function of the total occupancy, $\theta_t = \theta_1 + \theta_2$. (c) KMC simulation data (indicated by symbols) for the elements of the Λ_{ij} for binary mixtures as a function of the mole fraction, x_1, of component 1 in the adsorbed phase, keeping the total occupancy, $\theta_t = \theta_1 + \theta_2$ at a constant value of 0.48. The KMC data are normalized with respect to the unary diffusivity $Đ_1(0)$. The ratio of the unary diffusivities are $Đ_2(0)/Đ_1(0) = 8$. In (a) and (c), the value of the interaction energy, $w/RT = 0$; $\phi = 1$. In (b) the value of $\phi = 1.5$. The continuous solid lines are the calculations of the M–S model.

Combining Eqs. (13), (16), and (17) we obtain

$$\begin{pmatrix} N_1 \\ N_2 \end{pmatrix} = -\rho(1-\varepsilon)\,[\Lambda]\,[\Gamma] \begin{pmatrix} \frac{dq_1}{dz} \\ \frac{dq_2}{dz} \end{pmatrix};$$

$$\begin{pmatrix} N_1 \\ N_2 \end{pmatrix} = -\frac{\rho(1-\varepsilon)}{1+\frac{x_1 Đ_2}{Đ_{12}}+\frac{x_2 Đ_1}{Đ_{12}}} \begin{bmatrix} Đ_1\left(1+\frac{x_1 Đ_2}{Đ_{12}}\right) & \frac{x_1 Đ_1 Đ_2}{Đ_{12}} \\ \frac{x_2 Đ_1 Đ_2}{Đ_{12}} & Đ_2\left(1+\frac{x_2 Đ_1}{Đ_{12}}\right) \end{bmatrix} \begin{bmatrix} \Gamma_{11} & \Gamma_{12} \\ \Gamma_{21} & \Gamma_{22} \end{bmatrix} \begin{pmatrix} \frac{dq_1}{dz} \\ \frac{dq_2}{dz} \end{pmatrix} \quad (18)$$

The elements Λ_{ij} can be determined from MD or KMC simulations by monitoring molecule displacements; see Supplementary material for details. The Onsager Reciprocal Relation (ORR) impose the symmetry constraint $x_2\Lambda_{12} = x_1\Lambda_{21}$.

Fig. 3a presents KMC simulation data for Λ_{ij} for equimolar binary mixtures ($x_1 = x_2 = 0.5$), plotted as a function of the total occupancy, $\theta_t = \theta_1 + \theta_2$. The ratio of the unary diffusivities $Đ_2(0)/Đ_1(0) = 8$; the value of the interaction energy, $w/RT = 0$; $\phi = 1$. The continuous solid lines in Fig. 3a are based on Eq. (17) in which the M–S diffusivities are calculated $Đ_1$, and $Đ_2$ are calculated using Eq. (8), along with the interpolation formula (14), taking $\frac{Đ_i}{Đ_{ii}} = 0.9\theta_t$. There is excellent agreement between the KMC data and the estimations of the M–S model; this demonstrates the power of the M–S model to predict the characteristics of the surface diffusion of mixtures based on information on unary diffusivities. The same good agreement between KMC simulation data and the Maxwell–Stefan model holds for repulsive interactions between adjacent species, taking $\phi = 1.5$; see Fig. 3b.

For a more stringent test of the predictive capability of the M–S model, Fig. 3c presents comparison of the M–S model with KMC simulation data for the elements of the Λ_{ij} for binary mixtures as a function of the mole fraction, x_1, of component 1 in the adsorbed phase, keeping the total occupancy, $\theta_t = \theta_1 + \theta_2$ at a constant value of 0.48. The M–S model, along with the interpolation Formula (14) is able to provide good estimates of the elements of the Λ_{ij} over the entire composition range.

The good agreement between KMC simulation data and the M–S model holds also for other choices of the diffusivity ratios $Đ_2(0)/Đ_1(0) = 1, 2, 4, 16$, for scenarios assuming attractive ($\phi = 0.5$) or repulsive interactions ($\phi = 1.5, 2$); see KMC data in Figs. S7–S9 of the Supplementary material.

5. Steady-state surface fluxes, and permeation selectivities

For steady-state transfer across a distance δ, along the surface as indicated in Fig. 1, the surface fluxes N_i are obtained by solving the set of two coupled ordinary differential Eq. (18) for the following set of boundary conditions)

$$\text{upstream face}: \quad z = 0; \quad p_i = p_{i0}; \quad q_i = q_{i0}; \quad \theta_i = \theta_{i0};$$

$$\theta_V = \theta_{V0}$$

$$\text{downstream face}: \quad z = \delta; \quad p_i = p_{i\delta}; \quad q_i = q_{i\delta}; \quad \theta_i = \theta_{i\delta};$$

$$\theta_V = \theta_{V\delta}$$

A simple linearized approximation (Krishna, 2017), is sufficiently accurate for practical applications. In the linearized approximation, the two matrices $[\Lambda]$, and $[\Gamma]$ are assumed to be independent of compositions and loadings with values evaluated say at the upstream conditions. Alternatively, the two matrices $[\Lambda]$, and $[\Gamma]$ may be evaluated at the arithmetic averaged compositions across the diffusion path (Krishna, 2017). In this *linearized* model, the surface fluxes are calculated explicitly as follows

$$\begin{pmatrix} N_1 \\ N_2 \end{pmatrix} = \frac{\rho(1-\varepsilon)}{\delta} [\Lambda] [\Gamma] \begin{pmatrix} q_{10} - q_{1\delta} \\ q_{20} - q_{2\delta} \end{pmatrix} \tag{19}$$

In order to demonstrate the application of Eq. (19), we analyse the permeation of equimolar binary $CO_2(1)/CH_4(2)$ mixtures across a 2D pillared graphene surface, using the isotherm data of (Pedrielli et al., 2017). The ratio of the zero-loading M–S diffusivities is taken as $Đ_2(0)/Đ_1(0) = 2$. The calculations are presented in terms of the dimensionless fluxes $\frac{N_i\delta}{\rho(1-\varepsilon)Đ_1(0)q_{1,sat}}$; $i = 1, 2$; see Fig. 4a. The CO_2 flux is higher than that of CH_4 despite the fact that CH_4 is the more mobile species. The larger flux of CO_2 is due to two separate, and complimentary, reasons: (1) the mixture adsorption equilibrium favors CO_2, and (2) correlation effects tend to slow down the more mobile CH_4.

The continuous solid line in Fig. 4b is the permeation selectivities, S_{perm} calculated from

$$S_{perm} = \frac{N_1/N_2}{p_{10}/p_{20}} \tag{20}$$

The dashed lines are the calculations of the CO_2/CH_4 permeation selectivities using a scenario in which the slowing-down effects are ignored, i.e.

$$[\Lambda] = \begin{bmatrix} Đ_1 & 0 \\ 0 & Đ_2 \end{bmatrix} \tag{21}$$

Ignoring correlation effects underestimates the CO_2/CH_4 permeation selectivities by about 60%. Correlation and slowing-down effects cannot be neglected.

Fig. 5a presents the corresponding results for permeation selectivities for binary $CO_2(1)/N_2(2)$ mixtures; the ratio of the zero-loading M–S diffusivities is taken as $Đ_2(0)/Đ_1(0) = 4$. The permeation selectivities are strongly in favor of CO_2, and are in the range 10–100. Neglecting correlations, underestimates the selectivities by factor of about three.

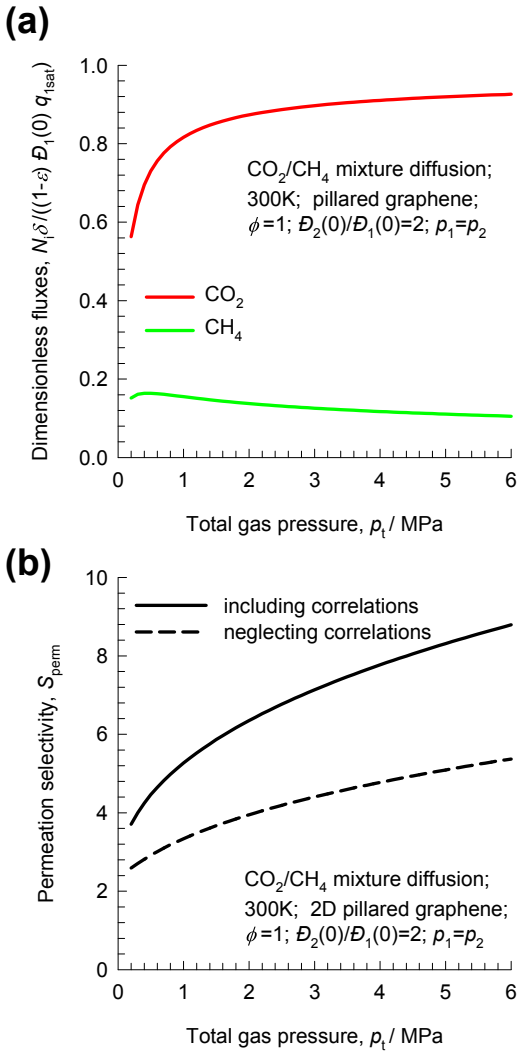

Fig. 4 – (a) Surface fluxes, and (b) permeation selectivities for permeation of binary $CO_2(1)/CH_4(2)$ mixtures across a 2D pillared graphene membrane at 300 K. The calculations are presented in terms of the dimensionless fluxes $\frac{N_i\delta}{\rho(1-\varepsilon)Đ_1(0)q_{1,sat}}$; $i = 1, 2$ for equimolar bulk fluid mixtures, with partial pressures $p_1 = p_2$. The ratio of the zero-loading M–S diffusivities is taken as $Đ_2(0)/Đ_1(0) = 2$. The interaction energies for both species are zero, i.e. $\phi = 1$ for both species. The input data are provided in the Supplementary material accompanying this publication.

Slowing-down effects become increasingly important if the differences in the mobilities are larger. As illustration, Fig. 5b; the ratio of the zero-loading M–S diffusivities is taken as $Đ_2(0)/Đ_1(0) = 10$; in this case, neglecting correlation effects underestimates the CO_2/H_2 permeation selectivities by about an order of magnitude. For permeation of $CH_4(1)/H_2(2)$ mixtures, neglecting correlation effects underestimates the CH_4/H_2 permeation selectivities by a factor of about three; see Fig. 5c.

In the four mixtures analyzed in Figs. 4 and 5 the surface transport of the more mobile species is hindered, i.e. slowed-down, by the tardier-more-strongly-adsorbed species. Our analysis quantifies the "inhibition" effect referred to by Wen et al. (2015).

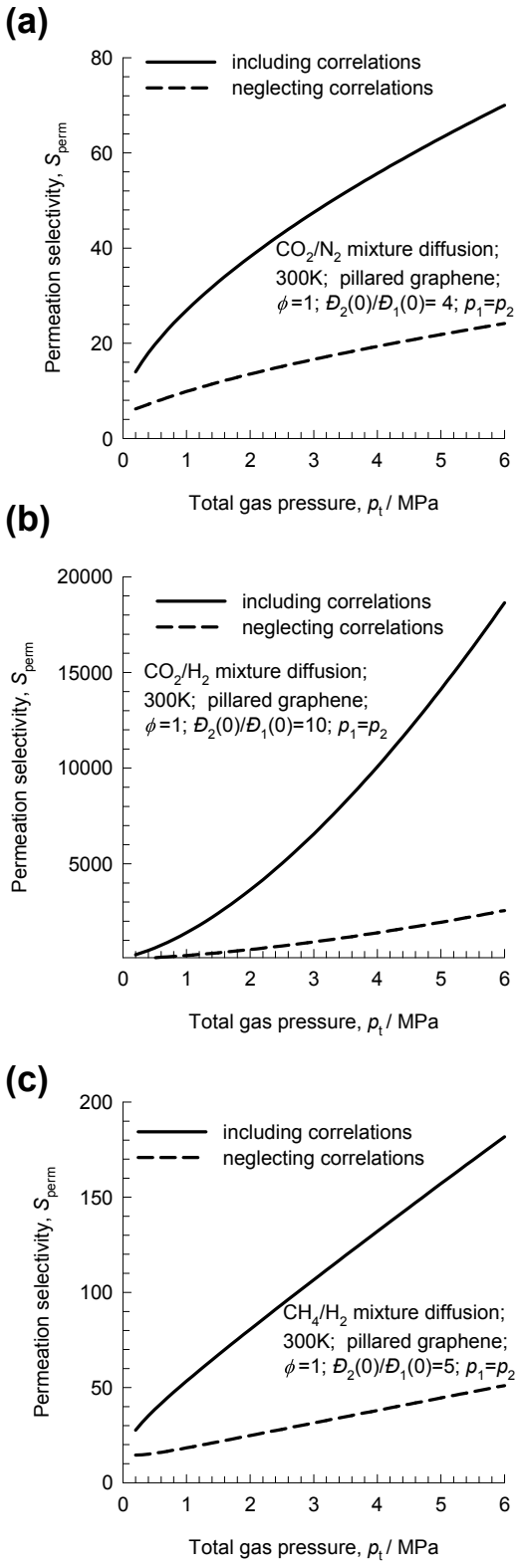

Fig. 5 – Selectivities for permeation of binary (a) $CO_2(1)/N_2(2)$, (b) $CO_2(1)/H_2(2)$, and (c) $CH_4(1)/H_2(2)$ mixtures across a 2D pillared graphene membrane at 300 K. The input data are provided in the Supplementary material accompanying this publication.

6. Applying the surface diffusion model in practice

For convenience of the readers we provide below a step-by-step methodology for practical application of the developed M–S model for mixture diffusion consisting of components 1 and 2.

The first step is to analyze the experimental data on unary isotherms using the QC theory; these isotherms are of vital importance in the analysis. By fitting Eq. (12) to the experimental unary isotherm data, the saturation capacity, along with the parameters b_i, and w can be determined; the procedure is outlined in the Supplementary material, and illustrated by the examples in Figs. S5–S7. With the information on the unary isotherms, the matrix of thermodynamic correction factors $[\Gamma]$ can be calculated using the Ideal Adsorbed Solution Theory.

The second step is to perform unary permeation experiments in order to back-out the zero-loading M–S diffusivities, $Đ_i(0)$. The loading dependence of the M–S diffusivities, $Đ_i$, can then be determined using Eqs. (8) and (9); these diffusivities will also hold for mixture diffusion.

The third step is to estimate the exchange coefficient $Đ_{12}$ using the interpolation Formula (14), wherein the self-exchange coefficients calculated from knowledge of the total mixture occupancy: $\theta_t = \theta_1 + \theta_2$ using the formula $\frac{Đ_i}{Đ_{ii}} = 0.9\theta_t$. For this purpose, we use the average of the occupancies in the upstream and downstream conditions.

The fourth step is the estimation of $[\Lambda]$ at the average occupancy with the aid of Eq. (17).

The final step is the explicit calculation of the permeation fluxes of components 1 and 2 using the linearized Eq. (19).

7. Conclusions

In this article, the Maxwell–Stefan (M–S) formulation has been used to model the surface diffusion of binary mixtures of adsorbates on 2D graphene surfaces. The characteristics of the M–S diffusivities were investigated with the aid of KMC simulations of unary and binary mixtures on a 2D square lattice of adsorption sites, taken as being representative of the graphene sheet. The following major conclusions can be drawn on the basis of the simulation results and analysis.

(1) The Reed–Ehrlich model, based on the quasi-chemical (QC) mean field approximation of Guggenheim, provides a convenient platform to quantify the loading dependence of the unary M–S diffusivities $Đ_1$ and $Đ_2$, characterizing the molecule-surface "friction". The model takes account of adsorbate–adsorbate interactions, either attractive or repulsive. In principle, the interaction energies can be determined from the unary adsorption isotherms.

(2) An important advantage of the M–S formulation is that the M–S diffusivities $Đ_i$ retain the same magnitude and characteristics for both unary diffusion and for diffusion in the presence of partner species. For binary mixture diffusion, the loading dependence of each of the M–S diffusivities $Đ_i$ is to be determined on the basis of the total mixture occupancy $\theta_t = \theta_1 + \theta_2$.

(3) The KMC simulations provide guidelines for estimation of the exchange coefficient, $Đ_{12}$, that quantifies *correlation*, or *slowing-down* effects for surface diffusion. The tardier-more-strongly-adsorbed species usually "slows down" the more-mobile-less-strongly-adsorbed species.

(4) Slowing-down effects become increasingly important with increasing differences in the adsorption strengths, and mobilities. For CO_2/CH_4, CO_2/H_2, CO_2/N_2, and CH_4/H_2, mixture separations, neglecting of slowing-down effects leads

to severe underestimations of the membrane permeation selectivities that favor the more strongly adsorbed species.

The next step in our investigation is the development of a more comprehensive model for mixture permeation that includes all of the individual steps shown in Fig. 1.

Appendix A. Supplementary data

Supplementary data associated with this article can be found, in the online version, at https://doi.org/10.1016/j.cherd.2018.03.033.

References

Blankenburg, S., Bieri, M., Fasel, R., Müllen, K., Pignedoli, C.A., Passerone, D., 2010. Porous graphene as an atmospheric nanofilter. Small 6, 2266–2271.

Celebi, K., Buchheim, J., Wyss, R.M., Droudian, A., Gasser, P., Shorubalko, I., Kye, J.-I., Lee, C., Park, H.G., 2014. Ultimate permeation across atomically thin porous graphene. Science 344, 289–292.

Drahushuk, L.W., Strano, M.S., 2012. Mechanisms of gas permeation through single layer graphene membranes. Langmuir 28, 16671–16678.

Du, H., Li, J., Zhang, J., Su, G., Li, X., Zhao, Y., 2011. Separation of hydrogen and nitrogen gases with porous graphene membrane. J. Phys. Chem. C 115, 23261–23266.

Gadipelli, S., Guo, Z.X., 2015. Graphene-based materials: synthesis and gas sorption storage and separation. Prog. Mater. Sci. 69, 1–60.

Hauser, A.W., Schwerdtfeger, P., 2012. Methane-selective nanoporous graphene membranes for gas purification. Phys. Chem. Chem. Phys. 14, 13292–13298.

Jiao, S., Xu, Z., 2015. Selective gas diffusion in graphene oxides membranes: a molecular dynamics simulations study. ACS Appl. Mater. Interfaces 7, 9052–9059.

Khakpay, A., Rahmani, F., Nouranian, S., Scovazzo, P., 2017. Molecular insights on the CH4/CO_2 separation in nanoporous graphene and graphene oxide separation platforms: adsorbents versus membranes. J. Phys. Chem. C. 121, 12308–12320.

Kim, H.W., Yoon, H.W., Yoon, S.-M., Yoo, B.M., Ahn, B.K., Cho, Y.H., Shin, H.J., Yang, H., Paik, U., Kwon, S., Choi, J.-Y., Park, H.B., 2013. Selective gas transport through few-layered graphene and graphene oxide membranes. Science 342, 91–95.

Knudsen, M., 1909. Die Gesetze der Molekularströmung und der inneren Reibungsströmung der Gase durch Röhren. Ann. Phys. 333, 75–130.

Koenig, S.P., Wang, L., Pellegrino, J., Bunch, J.S., 2012. Selective molecular sieving through porous graphene. Nat. Nanotechnol. 7, 728–732.

Krishna, R., 1990. Multicomponent surface diffusion of adsorbed species — a description based on the generalized Maxwell-Stefan equations. Chem. Eng. Sci. 45, 1779–1791.

Krishna, R., 2009. Describing the diffusion of guest molecules inside porous structures. J. Phys. Chem. C 113, 19756–19781.

Krishna, R., 2012. Diffusion in porous crystalline materials. Chem. Soc. Rev. 41, 3099–3118.

Krishna, R., 2014. The Maxwell-Stefan description of mixture diffusion in nanoporous crystalline materials. Microporous Mesoporous Mater. 185, 30–50.

Krishna, R., 2015. Uphill diffusion in multicomponent mixtures. Chem. Soc. Rev. 44, 2812–2836.

Krishna, R., 2016a. Diffusing uphill with James Clerk Maxwell and Josef Stefan. Curr. Opin. Chem. Eng. 12, 106–119.

Krishna, R., 2016b. Tracing the origins of transient overshoots for binary mixture diffusion in microporous crystalline materials. Phys. Chem. Chem. Phys. 18, 15482–15495.

Krishna, R., 2017. Using the Maxwell-Stefan formulation for highlighting the influence of interspecies (1-2) friction on binary mixture permeation across microporous and polymeric membranes. J. Membr. Sci. 540, 261–276.

Krishna, R., Paschek, D., Baur, R., 2004. Modelling the occupancy dependence of diffusivities in zeolites. Microporous Mesoporous Mater. 76, 233–246.

Krishna, R., van Baten, J.M., 2006. Describing binary mixture diffusion in carbon nanotubes with the Maxwell-Stefan equations. An investigation using molecular dynamics simulations. Ind. Eng. Chem. Res. 45, 2084–2093.

Krishna, R., van Baten, J.M., 2009a. Unified Maxwell-Stefan description of binary mixture diffusion in micro- and meso-porous materials. Chem. Eng. Sci. 64, 3159–3178.

Krishna, R., van Baten, J.M., 2009b. A molecular dynamics investigation of a variety of influences of temperature on diffusion in zeolites. Microporous Mesoporous Mater. 125, 126–134.

Krishna, R., van Baten, J.M., 2011. Maxwell-Stefan modeling of slowing-down effects in mixed gas permeation across porous membranes. J. Membr. Sci. 383, 289–300.

Krishna, R., van Baten, J.M., 2013a. Investigating the influence of diffusional coupling on mixture permeation across porous membranes. J. Membr. Sci. 430, 113–128.

Krishna, R., van Baten, J.M., 2013b. Influence of adsorption thermodynamics on guest diffusivities in nanoporous crystalline materials. Phys. Chem. Chem. Phys. 15, 7994–8016.

Li, H., Song, Z., Zhang, X., Huang, Y., Li, S., Mao, Y., Ploehn, H.J., Bao, Y., Yu, M., 2013. Ultrathin, molecular-sieving graphene oxide membranes for selective hydrogen separation. Science 342, 95–98.

Liu, G., Jin, W., Xu, N., 2015. Graphene-based membranes. Chem. Soc. Rev. 44, 5016–5030.

Myers, A.L., Prausnitz, J.M., 1965. Thermodynamics of mixed gas adsorption. AIChE J. 11, 121–130.

Nair, R.R., Wu, H.A., Jayaram, P.N., Grigorieva, I.V., Geim, A.K., 2012. Unimpeded permeation of water through helium-leak-tight graphene-based membranes. Science 335, 442–444.

Paschek, D., Krishna, R., 2000. Monte Carlo simulations of self- and transport-diffusivities of 2-methylhexane in silicalite. Phys. Chem. Chem. Phys. 2, 2389–2394.

Paschek, D., Krishna, R., 2001a. Diffusion of binary mixtures in zeolites: Kinetic Monte Carlo versus molecular dynamics simulations. Langmuir 17, 247–254.

Paschek, D., Krishna, R., 2001b. Kinetic Monte Carlo simulations of transport diffusivities of binary mixtures in zeolites. Phys. Chem. Chem. Phys. 3, 3185–3191.

Pedrielli, A., Taioli, S., Garberoglio, G., Pugno, N.M., 2017. Gas adsorption and dynamics in pillared graphene frameworks. Microporous Mesoporous Mater. 257, 222–231, http://dx.doi.org/10.1016/j.micromeso.2017.08.034.

Reed, D.A., Ehrlich, G., 1981. Surface diffusion, atomic jump rates and thermodynamics. Surf. Sci. 102, 588–609.

Schrier, J., 2012. Carbon dioxide separation with a two-dimensional polymer membrane. ACS Appl. Mater. Interfaces 4, 3745–3752.

Shan, M., Xue, Q., Jing, N., Ling, C., Zhang, T., Yan, Z., Zheng, J., 2012. Influence of chemical functionalization on the CO_2/N_2 separation performance of porous graphene membranes. Nanoscale 4, 5477–5482.

Solvik, K., Weaver, J.A., Brockway, A.M., Schrier, J., 2013. Entropy-driven molecular separations in 2D-nanoporous materials, with application to high-performance paraffin/olefin membrane separations. J. Phys. Chem. C 117, 17050–17057.

Sun, C., Bai, B., 2017a. Fast mass transport across two-dimensional graphene nanopores: nonlinear pressure-dependent gas permeation flux. Chem. Eng. Sci. 165, 186–191.

Sun, C., Bai, B., 2017b. Gas diffusion on graphene surfaces. Phys. Chem. Chem. Phys. 19, 3894–3902.

Sun, C., Boutilier, M.S.H., Au, H., Poesio, P., Bai, B., Karnik, R., Hadjiconstantinou, N.G., 2014. Mechanisms of molecular permeation through nanoporous graphene membranes. Langmuir 30, 675–682.

Vignes, A., 1966. Diffusion in binary solutions. Ind. Eng. Chem. Fundam. 5, 189–199.

Wang, L., Boutilier, M.S.H., Kidambi, P.R., Jang, D., Hadjiconstantinou, N.G., Karnik, R., 2017a. Fundamental transport mechanisms, fabrication and potential applications of nanoporous atomically thin membranes. Nat. Nanotechnol. 12, 509–522.

Wang, Q.H., Bellisario, D.O., Drahushuk, L.W., Jain, R.M., Kruss, S., Landry, M.P., Mahajan, S.G., Shimizu, S.F.E., Ulissi, Z.W., Strano, M.S., 2014. Low dimensional carbon materials for applications in mass and energy transport. Chem. Mater. 26, 172–183.

Wang, Y., Yang, Q., Zhong, C., Li, J., 2017b. Theoretical investigation of gas separation in functionalized nanoporous graphene membranes. Appl. Surf. Sci. 407, 532–539.

Wen, B., Sun, C., Bai, B., 2015. Inhibition effect of a non-permeating component on gas permeability of nanoporous graphene membranes. Phys. Chem. Chem. Phys. 17, 23619–23626.

Yuan, Z., Rajan, A.G., Misra, R.P., Drahushuk, L.W., Agrawal, K.V., Strano, M.S., Blankschtein, D., 2017. Mechanism and prediction of gas permeation through sub-nanometer graphene pores: comparison of theory and simulation. ACS Nano 11, 7974–7987.

Supplementary Material to accompany

The Maxwell-Stefan Description of Mixture Permeation across Nanoporous Graphene Membranes

Rajamani Krishna

Van 't Hoff Institute for Molecular Sciences, University of Amsterdam, Science Park 904,

1098 XH Amsterdam, The Netherlands

*Tel +31 20 6270990; Fax: + 31 20 5255604;

email: r.krishna@contact.uva.nl

Table of Contents

1. Preamble

This Supplementary material accompanying our manuscript *The Maxwell-Stefan Description of Mixture Permeation across Nanoporous Graphene Membranes* provides:

(a) Detailed derivation of the Maxwell-Stefan equations describing surface diffusion

(b) Data on unary isotherm fits used in the illustrative examples

For ease of reading, this Supplementary material is written as a stand-alone document. As a consequence, there is some overlap of material with the main manuscript.

2. The Maxwell-Stefan description of mixture diffusion on 2D surfaces

The primary focus is on the surface diffusion phenomenon shown in the schematic in Figure 1. The M-S equations represent a balance between the force exerted per mole of species *i* with the drag, or friction, experienced with each of the partner species in the mixture. We may expect that the frictional drag to be proportional to differences in the velocities of the diffusing species $\left(u_i - u_j\right)$, where u_i is the velocity of motion of the adsorbate on the 2D surface. For a mixture containing a total of *n* penetrants, 1, 2, 3,..*n* we write

$$-\frac{d\mu_i}{dz} = \sum_{j=1;j\neq i}^{n} \frac{RT}{Đ_{ij}} X_j\left(u_j - u_n\right) + \frac{RT}{Đ_{im}} X_m\left(u_i - u_m\right); \quad i = 1,2,..n \tag{1}$$

The left members of equation (1) are the negative of the gradients of the chemical potentials, with the units N mol^{-1}; it represents the driving force acting per mole of species *i*. The subscript m refers to the membrane, that is regarded as the (*n*+1)*th* component in the mixture; the membrane is considered to be stationary, i.e., $u_m = 0$. The term $RT/Đ_{im}$ is interpreted as the drag

or friction coefficient between the penetrant *i* and the membrane. The term $RT/Đ_{ij}$ is interpreted as the friction coefficient for the *i-j* pair of penetrants. The multiplier X_j in each of the right members represents a measure of the composition of component *j* in the adsorbed mixture because we expect the friction to be dependent on the number of molecules of *j* relative to that of component *i*. Since the composition fraction X_m of the 2D membrane is undefined, we redefine the M-S diffusivity for interaction of the penetrant *i* with the membrane as $Đ_i \equiv Đ_{im}/X_m$.

At the molecular level, the coefficients $Đ_{ij}$ reflect how the facility for transport of species *i* *correlates* with that of species *j*; they are also termed *exchange coefficients*. The inclusion of such correlation effects is vital because the tardier-more-strongly-adsorbed species usually "slows down" the more-mobile-less-strongly-adsorbed species, as shall be demonstrated later in this article.

If q_i is the molar loading of adsorbate *i*, expressed say as moles per kg of the graphene layer, and q_t is the total mixture loading $q_t = \sum_{i=1}^{n} q_i$, we may define the mole fractions of the components in the adsorbed phase, x_i:

$$x_i = q_i / q_t \tag{2}$$

In terms of mole fractions, equations (1) are modified as follows

$$-\frac{d\mu_i}{dz} = \sum_{j=1;j\neq i}^{n} \frac{RT}{Đ_{ij}} x_j \left(u_j - u_n\right) + \frac{RT}{Đ_i}\left(u_i\right); \quad i = 1,2,..n \tag{3}$$

The Maxwell-Stefan diffusion formulation (3) is consistent with the theory of irreversible thermodynamics; the Onsager Reciprocal Relations imply that the M-S pair diffusivities are symmetric

$$Đ_{ij} = Đ_{ji} \tag{4}$$

For uniformly spaced pores, each say of diameter d_{pore}, with inter-pore spacing L, the maximum distance to be traversed along the surface for any adsorbate is $\delta = \dfrac{\sqrt{2}L - d_{pore}}{2}$; see Figure 2. The area fraction of pores relative to the total membrane cross-sectional area is $\varepsilon = \dfrac{\pi d_{pore}^2/4}{L^2}$. The fractional area available for surface adsorption is $1-\varepsilon = 1 - \dfrac{\pi d_{pore}^2/4}{L^2}$. The membrane permeation flux, defined as the number of moles transported across the membrane per second per m^2 of total membrane surface area is

$$N_i \equiv (1-\varepsilon)\rho q_i u_i \tag{5}$$

In equation (5), ρ is the mass density of the graphene layer, expressed in the units of kg m^{-3}. Multiplying both sides of equation (3) by $(1-\varepsilon)q_i$, the M-S equations take the form[1-3]

$$-\rho(1-\varepsilon)\frac{q_i}{RT}\frac{d\mu_i}{dz} = \sum_{\substack{j=1 \\ j\neq i}}^{n} \frac{x_j N_i - x_i N_j}{Đ_{ij}} + \frac{N_i}{Đ_i}; \quad i = 1,2,..n \tag{6}$$

The chemical potential of component i in the adsorbed phase equals the chemical potential of that component in the bulk fluid mixture, i.e. $d\mu_i = RTd\ln f_i$, where f_i is the partial fugacity in the bulk fluid phase. The chemical potential gradients $d\mu_i/dz$ can be related to the gradients of the molar loadings, q_i, by defining thermodynamic correction factors Γ_{ij}

$$\frac{q_i}{RT}\frac{d\mu_i}{dz} = \sum_{j=1}^{n}\Gamma_{ij}\frac{dq_j}{dz}; \quad \Gamma_{ij} = \frac{q_i}{f_i}\frac{\partial f_i}{\partial q_j}; \quad i,j = 1,....n \tag{7}$$

The thermodynamic correction factors Γ_{ij} can be calculated by differentiation of the model describing mixture adsorption equilibrium, that relates the molar loadings, q_i, to the partial

fugacities in the bulk fluid mixture, f_i. Generally speaking, the Ideal Adsorbed Solution Theory (IAST) of Myers and Prausnitz [4] is the preferred method for estimation of mixture adsorption equilibrium.

In some special cases, the mixed-gas Langmuir model for ideal gas mixtures, with partial pressures, p_i

$$\theta_i = \frac{q_i}{q_{i,sat}} = \frac{b_i p_i}{1 + b_1 p_1 + b_2 p_2}; \quad i = 1,2 \tag{8}$$

may be of adequate accuracy. Analytic differentiation of equation (8) yields [5]

$$\begin{bmatrix} \Gamma_{11} & \Gamma_{12} \\ \Gamma_{21} & \Gamma_{22} \end{bmatrix} = \frac{1}{\theta_V} \begin{bmatrix} 1-\theta_2 & \frac{q_{1,sat}}{q_{2,sat}}\theta_1 \\ \frac{q_{2,sat}}{q_{1,sat}}\theta_2 & 1-\theta_1 \end{bmatrix} \tag{9}$$

where the fractional vacancy θ_V is defined as

$$\theta_V = 1 - \theta_1 - \theta_2 \tag{10}$$

Though a limited number of MD simulation data on *unary* self-diffusivities have been reported,[6-9] to our knowledge, there is no available MD or experimental data on the M-S diffusivities $Đ_i$, and $Đ_{ij}$ that are required in the use of equations (6) to calculate surface diffusion fluxes. The subsequent sections of this article address the following set of questions.

(1) Are the coefficients $Đ_i$ characterizing unary diffusion identifiable with those describing mixture diffusion?

(2) How do the M-S diffusivities $Đ_i$ depend on the molar loadings, q_i?

(3) How do adsorbate-adsorbate interactions influence the $Đ_i$?

(4) How do we predict the exchange coefficients $Đ_{ij}$?

(5) How do the exchange coefficients $Đ_{ij}$ influence the membrane separation selectivities?

3. Unary diffusion on a square array of adsorption sites

For the purposes of describing surface diffusion, the 2D surface may be viewed as consisting of a square array of adsorption sites; see schematic in Figure 3. A molecule, say species *i*, may hop from one site to an adjacent one, provided that site is vacant. In the simplest scenario, when there are no molecule-molecule interactions, either attractive or repulsive, the jump frequency ν_i is proportional to the fractional vacancy: $\nu_i = \nu_i(0)(1-\theta)$ where $\theta_i = q_i / q_{i,sat}$ is the fractional occupancy. In this scenario, the M-S diffusivity is a linearly decreasing function of occupancy

$$Đ_i = Đ_i(0)(1-\theta_i) \tag{11}$$

In equation (11), the M-S diffusivity in the limit of vanishingly small occupancies, $Đ_i(0) = \frac{1}{\zeta}\nu_i(0)\lambda^2$, where ζ is the coordination number of the lattice and λ is the jump distance on the square lattice; for a square lattice, $\zeta = 4$.

More generally, molecule-molecule interactions serve to influence the jump frequencies by a factor that depends on the energy of interaction, *w*. For repulsive interactions, $w > 0$, whereas for attractive interactions, $w < 0$. Using the quasi-chemical approach of Reed and Ehrlich[10] to quantify such interactions, the following expression is obtained for the loading dependence of the M-S diffusivities[11, 12]

$$Đ_i = Đ_i(0)\left(\frac{1+\beta_i}{2\,(1-\theta_i)}\right)^{-\zeta}\left(1+\frac{(\beta_i - 1 + 2\theta_i)\phi}{2\,(1-\theta_i)}\right)^{\zeta-1} \tag{12}$$

In equation (12) the following dimensionless parameters are defined

$$\beta_i = \sqrt{1 - 4\,\theta_i(1-\theta_i)(1-1/\phi)}; \quad \phi = \exp(w/RT) \tag{13}$$

In the limiting case of no interactions, $w = 0$, $\phi = 1$, $\beta_i = 1$ and equation (11) is recovered. The continuous solid lines in Figure 4a are the calculations of the occupancy dependence of the normalized M-S diffusivity using equations (12), and (13) for four different values of $\phi = \exp(w/RT) = 0,\ 0.5,\ 1.5,\ 2$. The symbols in Figure 4a are Kinetic Monte Carlo (KMC) simulation data for the M-S diffusivity, $Đ_i$, determined by monitoring the mean square displacement of an *ensemble* of molecules on a square lattice using the methodology described in detailed in our previous works[11, 13-15]

$$Đ_i = \frac{1}{\zeta}\lim_{\Delta t\to\infty}\frac{1}{n_i \Delta t}\left(\sum_{l=1}^{n_i}\left(\mathbf{r}_{l,i}(t+\Delta t) - \mathbf{r}_{l,i}(t)\right)\right)^2 \tag{14}$$

In equation (14), n_i is the number of molecules of species i in simulation box, and $\mathbf{r}_{l,i}(t)$ is the position vector for molecule l of species i at any time t, and Δt is the time interval for sampling.

There is excellent match between the KMC simulation data and the Reed-Ehrlich model calculations. In our previous work, using MD simulations, we had established the applicability of the Reed-Ehrlich model for diffusion of linear alkanes in carbon nanotubes.[16]

The symbols in Figure 4b are the simulation data for the self-diffusivities, $D_{i,self}$, determined by analyzing the mean square displacement of *individual* molecules

$$D_{i,self} = \frac{1}{\zeta}\lim_{\Delta t\to\infty}\frac{1}{n_i \Delta t}\sum_{l=1}^{n_i}\left(\mathbf{r}_{l,i}(t+\Delta t) - \mathbf{r}_{l,i}(t)\right)^2 \tag{15}$$

The self-diffusivities are generally lower than the corresponding values of the M-S diffusivities, i.e. $D_{i,self} < Đ_i$; the extent of lowering is due to *correlation* effects; a molecule may

jump to a site whence it originated. In order to derive the relation between the self-diffusivities and the M-S diffusivities, we apply equations (6) for a binary mixture consisting of tagged, or tracer, species (i*) and untagged species i that are otherwise identical. For equimolar diffusion, i.e. $N_i + N_{i^*} = 0$, equations (6) yield

$$-\rho(1-\varepsilon)\frac{q_i}{RT}\frac{d\mu_i}{dz} = \frac{(x_i + x_{i^*})N_i}{Đ_{ii}} + \frac{N_i}{Đ_i} = \left(\frac{1}{Đ_{ii}} + \frac{1}{Đ_i}\right)N_i \tag{16}$$

Equation (16) defines the self-diffusivity $D_{\mathrm{i,self}}$

$$-\rho(1-\varepsilon)\frac{q_i}{RT}\frac{d\mu_i}{dz} \equiv \frac{N_i}{D_{i,self}} \tag{17}$$

and we obtain

$$\frac{1}{D_{i,self}} = \frac{1}{Đ_i} + \frac{1}{Đ_{ii}} \tag{18}$$

We define the degree of correlations as

$$\frac{Đ_i}{Đ_{ii}} = \frac{Đ_i}{D_{i,self}} - 1 \tag{19}$$

The degree of correlations determined using equation (19) are plotted in Figure 4c as a function of the fractional occupancy; the dependence is nearly linear. It is interesting to note that correlation effects are practically uninfluenced by the interaction energies, and almost the entire data set lies within the narrow range; the value $\frac{Đ_i}{Đ_{ii}} = 0.9\theta_i$ is a fairly good representation of the entire data set.

For predicting the loading dependence of the M-S diffusivities, we clearly need good estimates of the interaction energies, w_{i}. In principle, this information can be extracted from the unary adsorption isotherms. Application of the quasi-chemical (QC) mean field approximation of

Guggenheim for adsorption on a lattice[17] yields the relation between the fugacity, f_i, in the gas phase and the fractional occupancy on the surface

$$b_i f_i = \frac{\theta_i}{(1-\theta_i)}\left(\frac{2\,(1-\theta_i)}{\beta_i + 1 - 2\theta_i}\right)^{\zeta} \tag{20}$$

In the limiting case of no interactions, $w = 0$, $\phi = 1$, $\beta_i = 1$, and equation (20) reduces to the Langmuir isotherm $b_i f_i = \frac{\theta_i}{(1-\theta_i)}$, where b_i is the Langmuir adsorption constant. By fitting experimental isotherm data to equation (20), we can determine $\phi = \exp(w/RT)$.

As illustration, Figures 5a,b,c,d present the experimental isotherm data of Zhang et al.[18] for unary isotherms of (a) CH_4, (b) C_2H_6, (c) C_3H_8, and (d) nC_4H_{10} for graphene sheets at $T = 283$ K, 293 K, and 303 K. The continuous solid lines represent calculations using equation (20) with fitted values of the parameters. $q_{i,sat}$, b_i, and w/RT for each guest at any T. For example at $T =$ 303 K, the energies of interaction for C_2H_6 are repulsive, whereas for nC_4H_{10}, the interactions are attractive.

Figure 6a compare the isotherm data of Sun and Bai[8] for CO_2 on a 2D graphene surface, obtained from molecular simulations, with calculations using equation (20), taking w/RT = -0.5, 0, 1. The best fit is achieved taking the interaction energy to be zero. Also, for CH_4 adsorption on graphene, the best fit is obtained taking w/RT = 0; see Figure 6b.

The unary isotherm data obtained from molecular simulations of Pedrielli et al.[19] for CO_2, CH_4, N_2, and H_2 on pillared graphene can also be fitted taking w/RT = 0; see Figure 7.

4. Surface diffusion of binary mixtures

For surface diffusion of binary mixtures, the Maxwell-Stefan equations (6) reduce to the set of two equations

$$\begin{aligned} -\rho(1-\varepsilon)\frac{q_1}{RT}\frac{d\mu_1}{dz} &= \frac{x_2 N_1 - x_1 N_2}{Đ_{12}} + \frac{N_1}{Đ_1} \\ -\rho(1-\varepsilon)\frac{q_2}{RT}\frac{d\mu_2}{\partial z} &= \frac{x_1 N_2 - x_2 N_1}{Đ_{12}} + \frac{N_2}{Đ_2} \end{aligned} \tag{21}$$

The first members on the right hand side of Equation (21) are required to quantify slowing-down effects that characterize binary mixture diffusion.[20-22] For a binary mixture, the exchange coefficient $Đ_{12}$ can be estimated by interpolating between the self-exchange coefficients of pure components: $Đ_{11}$ and $Đ_{22}$. On the basis of extensive MD data on mixture diffusivities in zeolites and MOFs the following interpolation formula, based on the Vignes[23] model for diffusion in liquid mixtures has been proposed[20, 21, 24]

$$Đ_{12} = \left(Đ_{11}\right)^{x_1}\left(Đ_{22}\right)^{x_2} \tag{22}$$

For surface diffusion on square lattices, the self-exchange coefficients are calculated on the basis of the information presented in Figure 4c, but based on the total occupancy, $\theta_t = \theta_1+\theta_2$ $\frac{Đ_i}{Đ_{ii}} = 0.9\theta_t$, and not the individual component occupancies.

Let us define the square matrix [B]

$$[B] = \begin{bmatrix} \frac{1}{Đ_1} + \frac{x_2}{Đ_{12}} & -\frac{x_1}{Đ_{12}} \\ -\frac{x_2}{Đ_{12}} & \frac{1}{Đ_2} + \frac{x_1}{Đ_{12}} \end{bmatrix} \tag{23}$$

Equation (21) can be re-cast into 2-dimensional matrix notation

$$-\rho(1-\varepsilon)\begin{pmatrix} \frac{q_1}{RT}\frac{d\mu_1}{dz} \\ \frac{q_2}{RT}\frac{d\mu_2}{dz} \end{pmatrix} = [B]\begin{pmatrix} N_1 \\ N_2 \end{pmatrix}; \quad \begin{pmatrix} N_1 \\ N_2 \end{pmatrix} = -(1-\varepsilon)[B]^{-1}\begin{pmatrix} \frac{q_1}{RT}\frac{d\mu_1}{dz} \\ \frac{q_2}{RT}\frac{d\mu_2}{dz} \end{pmatrix} \tag{24}$$

We define the square matrix $[\Lambda] \equiv [B]^{-1}$; The inverse of the square matrix $[B]$ can be obtained explicitly

$$[\Lambda] \equiv [B]^{-1} = \frac{1}{1+\frac{x_1 Đ_2}{Đ_{12}}+\frac{x_2 Đ_1}{Đ_{12}}}\begin{bmatrix} Đ_1\left(1+\frac{x_1 Đ_2}{Đ_{12}}\right) & \frac{x_1 Đ_1 Đ_2}{Đ_{12}} \\ \frac{x_2 Đ_1 Đ_2}{Đ_{12}} & Đ_2\left(1+\frac{x_2 Đ_1}{Đ_{12}}\right) \end{bmatrix} \tag{25}$$

Combining equations (21), (24), and (25) we obtain

$$\begin{pmatrix} N_1 \\ N_2 \end{pmatrix} = -\rho(1-\varepsilon)[\Lambda][\Gamma]\begin{pmatrix} \frac{dq_1}{dz} \\ \frac{dq_2}{dz} \end{pmatrix};$$

$$\begin{pmatrix} N_1 \\ N_2 \end{pmatrix} = -\frac{\rho(1-\varepsilon)}{1+\frac{x_1 Đ_2}{Đ_{12}}+\frac{x_2 Đ_1}{Đ_{12}}}\begin{bmatrix} Đ_1\left(1+\frac{x_1 Đ_2}{Đ_{12}}\right) & \frac{x_1 Đ_1 Đ_2}{Đ_{12}} \\ \frac{x_2 Đ_1 Đ_2}{Đ_{12}} & Đ_2\left(1+\frac{x_2 Đ_1}{Đ_{12}}\right) \end{bmatrix}\begin{bmatrix} \Gamma_{11} & \Gamma_{12} \\ \Gamma_{21} & \Gamma_{22} \end{bmatrix}\begin{pmatrix} \frac{dq_1}{dz} \\ \frac{dq_2}{dz} \end{pmatrix} \tag{26}$$

The elements Λ_{ij} can be determined from MD or KMC simulations using the formula

$$\Lambda_{ij} = \frac{1}{\zeta}\lim_{\Delta t\to\infty}\frac{1}{n_j}\frac{1}{\Delta t}\left\langle\left(\sum_{l=1}^{n_i}\left(\mathbf{r}_{l,i}(t+\Delta t)-\mathbf{r}_{l,i}(t)\right)\right)\bullet\left(\sum_{k=1}^{n_j}\left(\mathbf{r}_{k,j}(t+\Delta t)-\mathbf{r}_{k,j}(t)\right)\right)\right\rangle \tag{27}$$

In this expression n_j represent the number of molecules of species *j* in the simulation system, and $\mathbf{r}_{l,i}(t)$ is the position of molecule *l* of species *i* at any time *t*. For unary systems equation (27) degenerates to equation (14). The Onsager Reciprocal Relation (ORR) impose the symmetry constraint $x_2\Lambda_{12} = x_1\Lambda_{21}$.

Figures 8a,b,c,d,e present KMC simulation data for Λ_{ij} for equimolar binary mixtures ($x_1 = x_2 = 0.5$), plotted as a function of the total occupancy, $\theta_t = \theta_1 + \theta_2$. The ratio of the unary diffusivities $Đ_2(0)/Đ_1(0)$ are chosen equal to 1, 2, 4, 8 and 16; the KMC data are normalized with respect to the unary diffusivity $Đ_1(0)$. The value of the interaction energy, $w/RT = 0$; $\phi = 1$ in all five cases.

The continuous solid lines in Figure 8 are based on equation (25) in which the M-S diffusivities are calculated $Đ_1$, and $Đ_2$ are calculated using equation (12), along with the interpolation formula (22), together with $\frac{Đ_i}{Đ_{ii}} = 0.9\theta_t$. There is good agreement between the KMC data and the estimations of the M-S model in all five cases; this demonstrates the power of the M-S model to predict the characteristics of the surface diffusion of mixtures based on information on unary diffusivities.

For a more stringent test of the predictive capability of the M-S model, Figure 9 presents comparison of the M-S model with KMC simulation data for the elements of the Λ_{ij} for binary mixtures as a function of the mole fraction, x_1, of component 1 in the adsorbed phase, keeping the total occupancy, $\theta_t = \theta_1 + \theta_2$ at a constant value of 0.48. The ratio of the unary diffusivities are (a) $Đ_2(0)/Đ_1(0) = 1$, (b) $Đ_2(0)/Đ_1(0) = 2$, (c) $Đ_2(0)/Đ_1(0) = 4$, and (d) $Đ_2(0)/Đ_1(0) = 8$; the KMC data are normalized with respect to the unary diffusivity $Đ_1(0)$ and the value of the interaction energy, $w/RT = 0$; $\phi = 1$ in all four cases. The M-S model, along with the interpolation formula (22) is able to provide good estimates of the elements of the Λ_{ij} in all four cases.

In order to test the predictive capability of the M-S model for cases in which the interaction energies are finite, Figures 10a,b,c compares KMC simulation data for Λ_{ij} for equimolar binary mixtures ($x_1 = x_2 = 0.5$), plotted as a function of the total occupancy, $\theta_t = \theta_1 + \theta_2$ for three different choices of the interaction energies: (a) $\phi = \exp(w/RT) = 0.5$; (b) $\phi = \exp(w/RT) = 1.5$, and (c)

$\phi = \exp(w/RT) = 2$. In each of these three case studies, interaction energies apply equally for 1-1, 2-2, and 1-2 neighboring pairs. The continuous solid lines are the calculations of the M-S model; the agreement is good in all cases.

5. Steady-state surface fluxes, and permeation selectivities

For steady-state transfer across a distance $\delta = \frac{\sqrt{2}L - d_{pore}}{2}$, along the surface as indicated in Figure 1, the surface fluxes N_i are obtained by solving the set of two coupled ordinary differential equations (26) for the following set of boundary conditions)

$$\text{upstream face}: \; z = 0; \quad p_i = p_{i0}; \quad q_i = q_{i0}; \quad \theta_i = \theta_{i0}; \quad \theta_V = \theta_{V0}$$

$$\text{downstream face}: \; z = \delta; \quad p_i = p_{i\delta}; \quad q_i = q_{i\delta}; \quad \theta_i = \theta_{i\delta}; \quad \theta_V = \theta_{V\delta}$$

A simple linearized approximation,[25] is sufficiently accurate for practical applications. In the linearized approximation, the two matrices $[\Lambda]$, and $[\Gamma]$ are assumed to be independent of compositions and loadings with values evaluated say at the upstream conditions. Alternatively, the two matrices $[\Lambda]$, and $[\Gamma]$ may be evaluated at a suitably averaged compositions and loadings.[25] In this *linearized* model, the surface fluxes are calculated explicitly as follows

$$\begin{pmatrix} N_1 \\ N_2 \end{pmatrix} = \frac{\rho(1-\varepsilon)}{\delta}[\Lambda][\Gamma]\begin{pmatrix} q_{10} - q_{1\delta} \\ q_{20} - q_{2\delta} \end{pmatrix} \tag{28}$$

In order to demonstrate the application of equation (28), we calculate the permeation fluxes and selectivities for diffusion of binary $CO_2(1)/CH_4(2)$ mixtures on a 2D graphene surface, using the isotherm data of Sun and Bai.[8] The ratio of the zero-loading M-S diffusivities is taken as $Đ_2(0)/Đ_1(0) = 2$.

The calculations are presented in terms of the dimensionless fluxes $\frac{N_i\delta}{\rho(1-\varepsilon)Đ_1(0)q_{1,sat}}$; $i=1,2$ for equimolar bulk gas mixtures, with equal partial pressures $p_1=p_2$; see Figure 11a. The CO_2 flux is a factor higher than that of CH_4 despite the fact that CH_4 is the more mobile species. The larger flux of CO_2 is due to two separate, and complimentary, reasons: (1) the mixture adsorption equilibrium favors CO_2, and (2) correlation effects tend to slow down the more mobile CH_4. The corresponding values of the permeation selectivities, S_{perm}:

$$S_{perm}=\frac{N_1/N_2}{p_{10}/p_{20}} \tag{29}$$

are shown by the continuous solid line in Figure 11b. The dashed lines are the calculations of the CO_2/CH_4 permeation selectivities using a scenario in which the slowing-down effects are ignored, i.e.

$$[\Lambda]=\begin{bmatrix} Đ_1 & 0 \\ 0 & Đ_2 \end{bmatrix} \tag{30}$$

and the permeation fluxes are calculated using

$$\begin{pmatrix} N_1 \\ N_2 \end{pmatrix}=\frac{\rho(1-\varepsilon)}{\delta}\begin{bmatrix} Đ_1 & 0 \\ 0 & Đ_2 \end{bmatrix}\begin{bmatrix} \Gamma_{11} & \Gamma_{12} \\ \Gamma_{21} & \Gamma_{22} \end{bmatrix}\begin{pmatrix} q_{10}-q_{1\delta} \\ q_{20}-q_{2\delta} \end{pmatrix} \tag{31}$$

Ignoring correlation effects underestimates the CO_2/CH_4 permeation selectivities by about 30%. Correlation and slowing-down effects cannot be neglected.

Slowing-down effects become increasingly important if the differences in the adsorption strengths are larger. To demonstrate this, Figure 12a presents calculations of the surface fluxes fordiffusion of binary CO_2/CH_4 mixtures on a 2D pillared graphene surface at 300 K, using the isotherm data of Pedrielli et al.[19] The ratio of the zero-loading M-S diffusivities is taken as

$Đ_2(0)/Đ_1(0) = 2$. Due to stronger adsorption, the CO_2/CH_4 permeation selectivities are strongly in favor of CO_2. In this case, neglecting correlation effects underestimates the CO_2/CH_4 permeation selectivities by about 60%.

Figure 13 presents the corresponding results for surface fluxes, and permeation selectivities for diffusion of binary $CO_2(1)/N_2(2)$ mixtures on a 2D pillared graphene surface at 300 K. The ratio of the zero-loading M-S diffusivities is taken as $Đ_2(0)/Đ_1(0) = 4$. The permeation selectivities are strongly in favor of CO_2, and are in the range 10 – 100. Neglecting correlations, underestimates the selectivities by factor of about three.

Slowing-down effects are also of significant importance if the differences in the mobilities are larger. As illustration, Figures 14a,b present the permeation fluxes, and permeation selectivities for diffusion of binary CO_2/H_2 mixture on a 2D pillared graphene surface at 300 K using the isotherm data of Pedrielli et al.[19] The ratio of the zero-loading M-S diffusivities is taken as $Đ_2(0)/Đ_1(0) = 10$. In this case, neglecting correlation effects underestimates the CO_2/H_2 permeation selectivities by about an order of magnitude.

Figures 15a,b present the corresponding results for surface fluxes, and selectivities for diffusion of binary $CH_4(1)/H_2(2)$ mixtures on a 2D pillared graphene surface at 300 K. In this case, neglecting correlation effects underestimates the CH_4/H_2 permeation selectivities by a factor of about three.

6. Entropy effects for permeation across graphene membranes

For mixture adsorption at high pressures, entropy effects favor the component with the higher saturation capacity; see published works.[26, 27] As illustration of entropy effects, we consider the permeation of $C_3H_8(1)/nC_4H_{10}(2)$ mixtures across a graphene membrane at 283 K. The unary isotherm fit parameters are provided by Zhang et al.[18] From the QC isotherm fits in Figures 5, we

conclude that both C3 and nC4 exhibit repulsive interactions. For use in the Reed-Ehrlich model, we use $\phi = \exp(w/RT)$ = 1.5. With increasing pressures, entropy effects favor the adsorption of the smaller C3 that has the higher saturation capacity. This implies that with in

Figure 16a presents a plot of the dimensionless surface fluxes $\frac{N_i \delta}{\rho(1-\varepsilon)Đ_1(0)q_{1,sat}}$; $i = 1,2$ for equimolar bulk fluid mixtures, with partial pressures p_1=p_2. With increasing total pressure p_t= p_1=p_2, we note that there is a significant increase in the C3 flux whereas the nC4 flux tends to reach a plateau value. The permeation selectivity (cf. Figure 16b) becomes increasingly in favor of C3. In this case, correlation effects tend to lower the permeation selectivity due to slowing-down effects.

7. Notation

b_i	parameter in the pure component Langmuir adsorption isotherm, Pa^{-1}
$[B]$	matrix of inverse Maxwell-Stefan coefficients, m^{-2} s
d_{pore}	pore diameter, m
$Đ_i$	M-S diffusivity of component i for molecule-surface interactions, m^2 s^{-1}
$Đ_i(0)$	M-S diffusivity at zero-loading, m^2 s^{-1}
$Đ_{ij}$	M-S exchange coefficient, m^2 s^{-1}
$Đ_{12}$	M-S exchange coefficient for binary mixture, m^2 s^{-1}
$D_{i,self}$	self-diffusivity of species i, m^2 s^{-1}
f_i	partial fugacity of species i, Pa
L	inter-pore spacing on graphene layer, m
N_i	molar flux of species i, mol m^{-2} s^{-1}
n	number of penetrants, dimensionless
n_i	number of molecules of species i in simulation box, dimensionless
p_i	partial pressure of species i, Pa
p_t	total system pressure, Pa
q_i	molar loading of species i, mol kg^{-1}
$q_{i,sat}$	molar loading of species i at saturation, mol kg^{-1}
q_t	total molar loading of mixture, mol kg^{-1}
$\mathbf{r}_{l,i}(t)$	position vector for molecule l of species i at any time t, m
R	gas constant, 8.314 J mol^{-1} K^{-1}
T	absolute temperature, K
u_i	velocity of motion of i, m s^{-1}
w	energy of interaction, J mol^{-1}

x_i	mole fraction of species *i* in adsorbed phase, dimensionless
z	distance coordinate, m

Greek letters

β	parameter defined in equation (13), dimensionless
Γ_{ij}	thermodynamic factors, dimensionless
$[\Gamma]$	matrix of thermodynamic factors, dimensionless
δ	diffusion distance as indicated in Figure 2, m
ε	fractional pore area relative to membrane area, dimensionless
ζ	coordination number, dimensionless
η	dimensionless distance, dimensionless
θ_i	fractional occupancy of component *i*, dimensionless
θ_t	fractional occupancy of adsorbed mixture, dimensionless
θ_V	fractional vacancy, dimensionless
λ	jump distance on 2D lattice, m
$[\Lambda]$	matrix of Maxwell-Stefan diffusivities, $m^2\ s^{-1}$
μ_i	molar chemical potential, $J\ mol^{-1}$
ν	jump frequency, s^{-1}
ϕ	parameter defined in equation (13), dimensionless
ρ	mass density of graphene layer, $kg\ m^{-3}$

Subscripts

1	referring to species 1
2	referring to species 2

i,j	components in mixture
i	referring to component *i*
t	referring to total mixture
sat	referring to saturation conditions
V	vacancy

Vector and Matrix Notation

( )	component vector
[ ]	square matrix

8. References

(1) Krishna, R. The Maxwell-Stefan Description of Mixture Diffusion in Nanoporous Crystalline Materials. *Microporous Mesoporous Mater.* **2014**, *185*, 30-50.

(2) Krishna, R.; van Baten, J. M. Maxwell-Stefan modeling of slowing-down effects in mixed gas permeation across porous membranes. *J. Membr. Sci.* **2011**, *383*, 289-300.

(3) Krishna, R. Tracing the Origins of Transient Overshoots for Binary Mixture Diffusion in Microporous Crystalline Materials. *Phys. Chem. Chem. Phys.* **2016**, *18*, 15482-15495.

(4) Myers, A. L.; Prausnitz, J. M. Thermodynamics of Mixed Gas Adsorption. *A.I.Ch.E.J.* **1965**, *11*, 121-130.

(5) Krishna, R.; Baur, R. Modelling Issues in Zeolite Based Separation Processes. *Sep. Purif. Technol.* **2003**, *33*, 213-254.

(6) Jiao, S.; Xu, Z. Selective Gas Diffusion in Graphene Oxides Membranes: A Molecular Dynamics Simulations Study. *ACS Appl. Mater. Interfaces* **2015**, *7*, 9052-9059.

(7) Sun, C.; Boutilier, M. S. H.; Au, H.; Poesio, P.; Bai, B.; Karnik, R.; Hadjiconstantinou, N. G. Mechanisms of Molecular Permeation through Nanoporous Graphene Membranes. *Langmuir* **2014**, *30*, 675-682.

(8) Sun, C.; Bai, B. Gas diffusion on graphene surfaces. *Phys. Chem. Chem. Phys.* **2017**, *19*, 3894-3902.

(9) Sun, C.; Bai, B. Fast Mass Transport across Two-Dimensional Graphene Nanopores: Nonlinear Pressure-Dependent Gas Permeation Flux. *Chem. Eng. Sci.* **2017**, *165*, 186-191.

(10) Reed, D. A.; Ehrlich, G. Surface diffusion, atomic jump rates and thermodynamics. *Surf. Sci.* **1981**, *102*, 588-609.

(11) Krishna, R.; Paschek, D.; Baur, R. Modelling the occupancy dependence of diffusivities in zeolites. *Microporous Mesoporous Mater.* **2004**, *76*, 233-246.

(12) Krishna, R.; van Baten, J. M. A molecular dynamics investigation of a variety of influences of temperature on diffusion in zeolites. *Microporous Mesoporous Mater.* **2009**, *125*, 126-134.

(13) Paschek, D.; Krishna, R. Monte Carlo simulations of self- and transport-diffusivities of 2-methylhexane in silicalite. *Phys. Chem. Chem. Phys.* **2000**, *2*, 2389-2394.

(14) Paschek, D.; Krishna, R. Kinetic Monte Carlo simulations of transport diffusivities of binary mixtures in zeolites. *Phys. Chem. Chem. Phys.* **2001**, *3*, 3185-3191.

(15) Paschek, D.; Krishna, R. Diffusion of binary mixtures in zeolites: Kinetic Monte Carlo versus molecular dynamics simulations. *Langmuir* **2001**, *17*, 247-254.

(16) Krishna, R.; van Baten, J. M. Describing binary mixture diffusion in carbon nanotubes with the Maxwell-Stefan equations. An investigation using molecular dynamics simulations. *Ind. Eng. Chem. Res.* **2006**, *45*, 2084-2093.

(17) Krishna, R.; van Baten, J. M. Influence of Adsorption Thermodynamics on Guest Diffusivities in Nanoporous Crystalline Materials. *Phys. Chem. Chem. Phys.* **2013**, *15*, 7994-8016.

(18) Zhang, X.; Sun, Y.; Su, W.; Wang, X. Adsorption Equilibria of C1−C4 from Natural Gas on Graphene Sheets. *J. Chem. Eng. Data* **2016**, *61*, 1667-1675.

(19) Pedrielli, A.; Taioli, S.; Garberoglio, G.; Pugno, N. M. Gas Adsorption and Dynamics in Pillared Graphene Frameworks. *Microporous Mesoporous Mater.* **2017**, *257*, 222-231. DOI:10.1016/j.micromeso.2017.08.034.

(20) Krishna, R. Describing the Diffusion of Guest Molecules inside Porous Structures. *J. Phys. Chem. C* **2009**, *113*, 19756-19781.

(21) Krishna, R. Diffusion in Porous Crystalline Materials. *Chem. Soc. Rev.* **2012**, *41*, 3099-3118.

(22) Krishna, R.; van Baten, J. M. Investigating the Influence of Diffusional Coupling on Mixture Permeation across Porous Membranes *J. Membr. Sci.* **2013**, *430*, 113-128.

(23) Vignes, A. Diffusion in binary solutions. *Ind. Eng. Chem. Fundamentals* **1966**, *5*, 189-199.

(24) Krishna, R.; van Baten, J. M. Unified Maxwell-Stefan Description of Binary Mixture Diffusion in Micro- and Meso- Porous Materials. *Chem. Eng. Sci.* **2009**, *64*, 3159-3178.

(25) Krishna, R. Using the Maxwell-Stefan formulation for Highlighting the Influence of Interspecies (1-2) Friction on Binary Mixture Permeation across Microporous and Polymeric Membranes. *J. Membr. Sci.* **2017**, *540*, 261-276.

(26) Krishna, R. Separating Mixtures by Exploiting Molecular Packing Effects in Microporous Materials. *Phys. Chem. Chem. Phys.* **2015**, *17*, 39-59.

(27) Krishna, R.; van Baten, J. M. Commensurate-Incommensurate Adsorption and Diffusion in Ordered Crystalline Microporous Materials. *Phys. Chem. Chem. Phys.* **2017**, *19*, 20320-20337.

(28) Drahushuk, L. W.; Strano, M. S. Mechanisms of Gas Permeation through Single Layer Graphene Membranes. *Langmuir* **2012**, *28*, 16671-16678.

9. Captions for Figures

Figure 1. Schematic showing transport mechanisms across 2D graphene membrane. Implicit in this schematic is that the inter-pore spacing is significantly larger than the length scale characteristics of surface diffusion; see Drahushuk and Strano.[28]

Figure 2. Schematic showing inter-pore spacing and diffusion distances.

Figure 3. Two-dimensional array of adsorption sites representing the 2D graphene surface.

Figure 4. KMC simulations (symbols) of normalized (a) Maxwell-Stefan and (b) self-diffusivities on a square lattice, plotted as a function of the fractional occupancy for four different values of $\phi = \exp(w/RT)$ = 0, 0.5, 1.5, 2. The continuous solid lines are the calculations using equations (12), and (13). (c) The degree of correlations $Đ_1/Đ_{11}$ plotted as a function of the fractional occupancy.

Figure 5. Experimental isotherm data of Zhang et al.[18] for unary isotherms of (a) CH_4, (b) C_2H_6, (c) C_3H_8, and (d) nC_4H_{10} for graphene sheets at T = 283 K, 293 K, and 303 K. The continuous solid lines represent calculations using equation (20).

Figure 6. Isotherm data obtained from molecular simulations for (a) CO_2, and (b) CH_4 on a 2D graphene (data scanned from Figure 3 of Sun and Bai[8]). The continuous solid lines represent calculations using equation (20): (a) taking w/RT = -0.5, 0, 1; saturation capacity, $q_{i,sat}$ = 9.6 molecules nm^{-2}; $b_i = 2.62\times10^{-7}$ Pa^{-1}, (b) taking w/RT = 0; the saturation capacity, $q_{i,sat}$ = 9.6 molecules nm^{-2}; $b_i = 7.67\times10^{-8}$ Pa^{-1}.

Figure 7. Isotherm data obtained from molecular simulations for CO_2, CH_4, N_2, and H_2 on pillared graphene (data scanned from Figures S37, S39, and S40 of the Supplementary material accompany the paper of Pedrielli et al.[19] for Pillar Type 4, with pillar density of 1.37 pillars nm^2) The continuous solid lines represent calculations using equation (20)taking w/RT = 0; and CO_2: saturation capacity, $q_{i,sat}$ = 8 mol kg^{-1}; $b_i = 1.5\times10^{-5}$ Pa^{-1}; CH_4: saturation capacity, $q_{i,sat}$ = 6 mol kg^{-1}; $b_i = 4\times10^{-6}$ Pa^{-1}; N_2: saturation capacity, $q_{i,sat}$ = 5 mol kg^{-1}; $b_i = 1\times10^{-6}$ Pa^{-1}; H_2: saturation capacity, $q_{i,sat}$ = 3.1 mol kg^{-1}; $b_i = 1\times10^{-7}$ Pa^{-1}.

Figure 8. KMC simulation data (indicated by symbols) for the elements of the Λ_{ij} for equimolar binary mixtures ($x_1 = x_2 = 0.5$), plotted as a function of the total occupancy, $\theta_t = \theta_1 + \theta_2$. The KMC data are normalized with respect to the unary diffusivity $Đ_1(0)$. The ratio of the unary diffusivities are (a) $Đ_2(0)/Đ_1(0) = 1$, (b) $Đ_2(0)/Đ_1(0) = 2$, (c) $Đ_2(0)/Đ_1(0) = 4$, (d) $Đ_2(0)/Đ_1(0) = 8$, and (e) $Đ_2(0)/Đ_1(0) = 16$. The value of the interaction energy, $w/RT = 0$; $\phi = 1$ in all five cases. The continuous solid lines are the calculations of the M-S model.

Figure 9. KMC simulation data (indicated by symbols) for the elements of the Λ_{ij} for binary mixtures as a function of the mole fraction, x_1, of component 1 in the adsorbed phase, keeping the total occupancy, $\theta_t = \theta_1 + \theta_2$ at a constant value of 0.48. The KMC data are normalized with respect to the unary diffusivity $Đ_1(0)$. The ratio of the unary diffusivities are (a) $Đ_2(0)/Đ_1(0) = 1$, (b) $Đ_2(0)/Đ_1(0) = 2$, (c) $Đ_2(0)/Đ_1(0) = 4$, and (d) $Đ_2(0)/Đ_1(0) = 8$. The value of the interaction energy, $w/RT = 0$; $\phi = 1$ in all four cases. The continuous solid lines are the calculations of the M-S model.

Figure 10. KMC simulation data (indicated by symbols) for the elements of the Λ_{ij} for equimolar binary mixtures ($x_1 = x_2 = 0.5$), plotted as a function of the total occupancy, $\theta_t = \theta_1 + \theta_2$. The KMC data are normalized with respect to the unary diffusivity $Đ_1(0)$. (a) $\phi = \exp(w/RT) = 0.5$, $Đ_2(0)/Đ_1(0) = 8$; (b) $\phi = \exp(w/RT) = 1.5$, $Đ_2(0)/Đ_1(0) = 8$; (c) $\phi = \exp(w/RT) = 2$, $Đ_2(0)/Đ_1(0) = 2$. The continuous solid lines are the calculations of the M-S model.

Figure 11. (a) Surface fluxes, and (b) permeation selectivities for permeation of binary $CO_2(1)/CH_4(2)$ mixtures across a 2D graphene membrane at 300 K. The calculations are presented in terms of the dimensionless fluxes $\frac{N_i\delta}{\rho(1-\varepsilon)Đ_1(0)q_{1,sat}}$; $i=1,2$ for equimolar bulk fluid mixtures, with partial pressures $p_1=p_2$. The ratio of the zero-loading M-S diffusivities is taken as $Đ_2(0)/Đ_1(0) = 2$. The interaction energies for both species are zero, i.e. $\phi = 1$ for both species. The unary isotherm fit parameters are specified in the legend to Figure 6. The mixture adsorption equilibrium was calculated using the mixed-gas Langmuir model because it is applicable for mixtures with equal saturation capacities.

Figure 12. (a) Surface fluxes, and (b) permeation selectivities for permeation of binary $CO_2(1)/CH_4(2)$ mixtures across a 2D pillared graphene membrane at 300 K. The calculations are presented in terms of the dimensionless fluxes $\frac{N_i\delta}{\rho(1-\varepsilon)Đ_1(0)q_{1,sat}}$; $i=1,2$ for equimolar bulk fluid mixtures, with partial pressures $p_1=p_2$. The ratio of the zero-loading M-S diffusivities is taken as $Đ_2(0)/Đ_1(0) = 2$. The interaction energies for both species are zero, i.e. $\phi = 1$ for both species. The unary isotherm fit parameters are specified in the legend to Figure 7. The mixture adsorption equilibrium was calculated using the IAST.

Figure 13. (a) Surface fluxes, and (b) permeation selectivities for permeation of binary $CO_2(1)/N_2(2)$ mixtures across a 2D pillared graphene membrane at 300 K. The calculations are presented in terms of the dimensionless fluxes $\frac{N_i\delta}{\rho(1-\varepsilon)Đ_1(0)q_{1,sat}}$; $i=1,2$ for equimolar bulk fluid mixtures, with partial pressures $p_1=p_2$. The ratio of the zero-loading M-S diffusivities is taken as $Đ_2(0)/Đ_1(0) = 4$. The interaction energies for both species are zero, i.e. $\phi = 1$ for both species. The unary isotherm fit parameters are specified in the legend to Figure 7. The mixture adsorption equilibrium was calculated using the IAST.

Figure 14. (a) Surface fluxes, and (b) permeation selectivities for permeation of binary $CO_2(1)/H_2(2)$ mixtures across 2D pillared graphene membrane at 300 K. The calculations are presented in terms of the dimensionless fluxes $\frac{N_i\delta}{\rho(1-\varepsilon)Đ_1(0)q_{1,sat}}$; $i=1,2$ for equimolar bulk fluid mixtures, with partial pressures $p_1=p_2$. The ratio of the zero-loading M-S diffusivities is taken as $Đ_2(0)/Đ_1(0) = 10$. The interaction energies for both species are zero, i.e. $\phi = 1$ for both species. The unary isotherm fit parameters are specified in the legend to Figure 7. The mixture adsorption equilibrium was calculated using the IAST.

Figure 15. (a) Surface fluxes, and (b) permeation selectivities for permeation of binary $CH_4(1)/H_2(2)$ mixtures across a 2D pillared graphene membrane at 300 K. The calculations are presented in terms of the dimensionless fluxes $\frac{N_i\delta}{\rho(1-\varepsilon)Đ_1(0)q_{1,sat}}$; $i=1,2$ for equimolar bulk

fluid mixtures, with partial pressures p_1=p_2. The ratio of the zero-loading M-S diffusivities is taken as $Đ_2(0)/Đ_1(0)$ = 5. The interaction energies for both species are zero, i.e. ϕ = 1 for both species. The unary isotherm fit parameters are specified in the legend to Figure 7. The mixture adsorption equilibrium was calculated using the IAST.

Figure 16. (a) Surface fluxes, and (b) permeation selectivities for permeation of binary C_3H_8(1)/ nC_4H_{10}(2) mixtures across a graphene membrane at 283 K. The calculations are presented in terms of the dimensionless fluxes $\frac{N_i\delta}{\rho(1-\varepsilon)Đ_1(0)q_{1,sat}}$; $i=1,2$ for equimolar bulk fluid mixtures, with partial pressures p_1=p_2. The ratio of the zero-loading M-S diffusivities is taken as $Đ_1(0)/Đ_2(0)$ = 2. The interaction energies for both species are $\phi=\exp(w/RT)$ = 1.5. The unary isotherm fit parameters are provided by Zhang et al.[18] The mixture adsorption equilibrium was calculated using the IAST.

Fig. S1

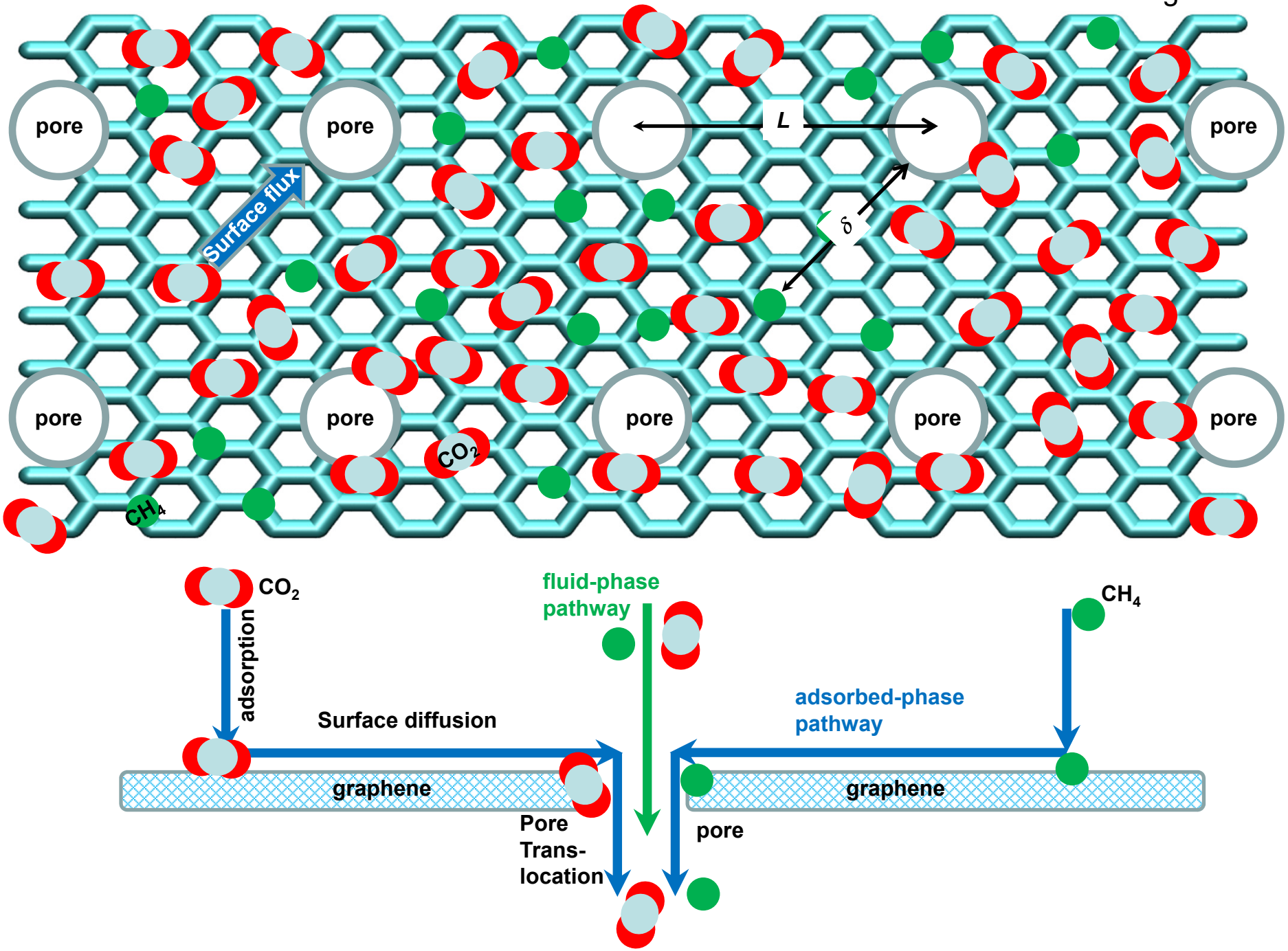
pore
pore
pore
pore
pore
pore
pore
pore
L
δ
Surface flux
CO2
CH4
CO2
adsorption
Surface diffusion
graphene
Pore
Trans-
location
fluid-phase
pathway
CH4
adsorbed-phase
pathway
graphene
pore

Fig. S2

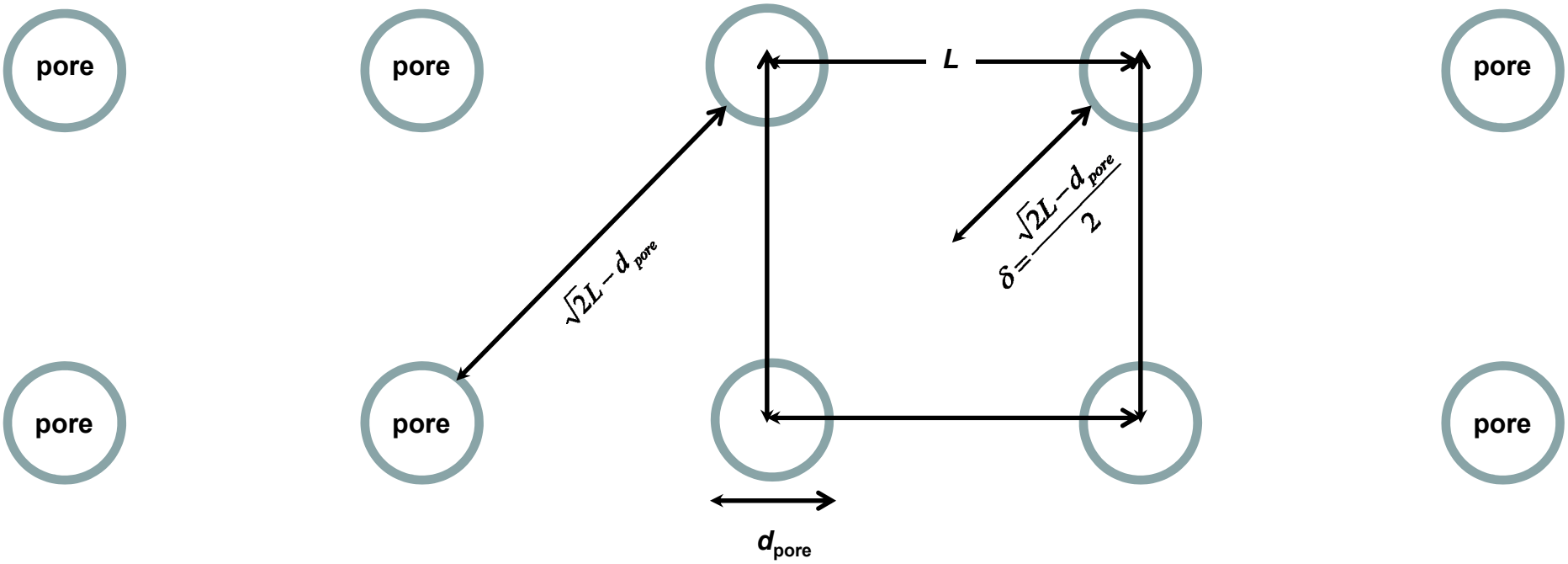
pore
pore
pore
pore
pore
pore
L
$\sqrt{2}L - d_{pore}$
$\delta = \frac{\sqrt{2}L - d_{pore}}{2}$
d_{pore}

KMC methodology

Fig. S3

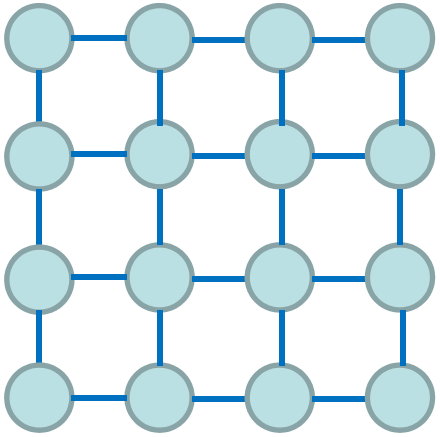

Unary diffusivities: KMC simulations vs Reed-Ehrlich

Fig. S4

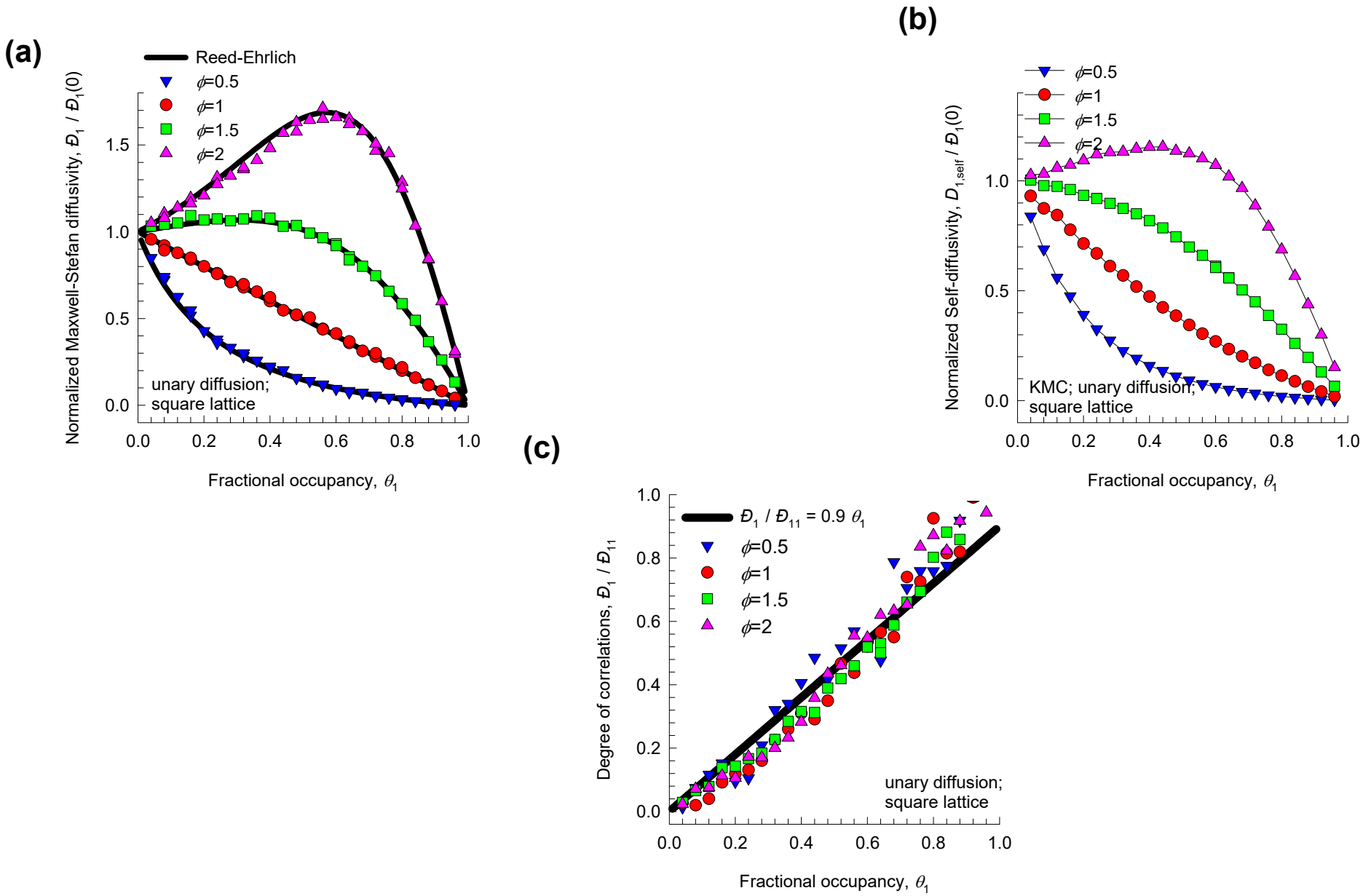

Fig. S5

Isotherm fitting to determine interaction energies

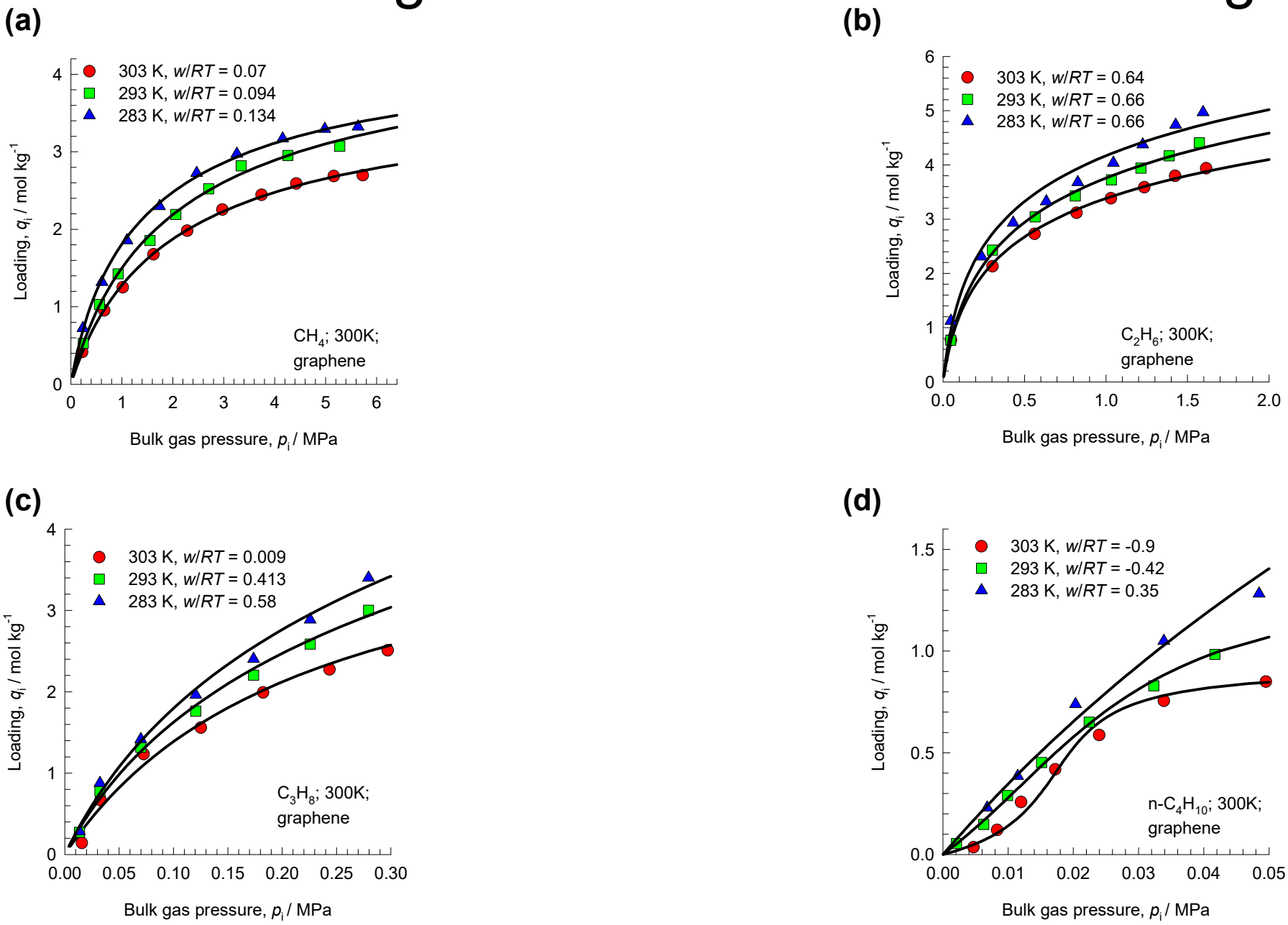

Fig. S6

Isotherm fitting to determine interaction energies

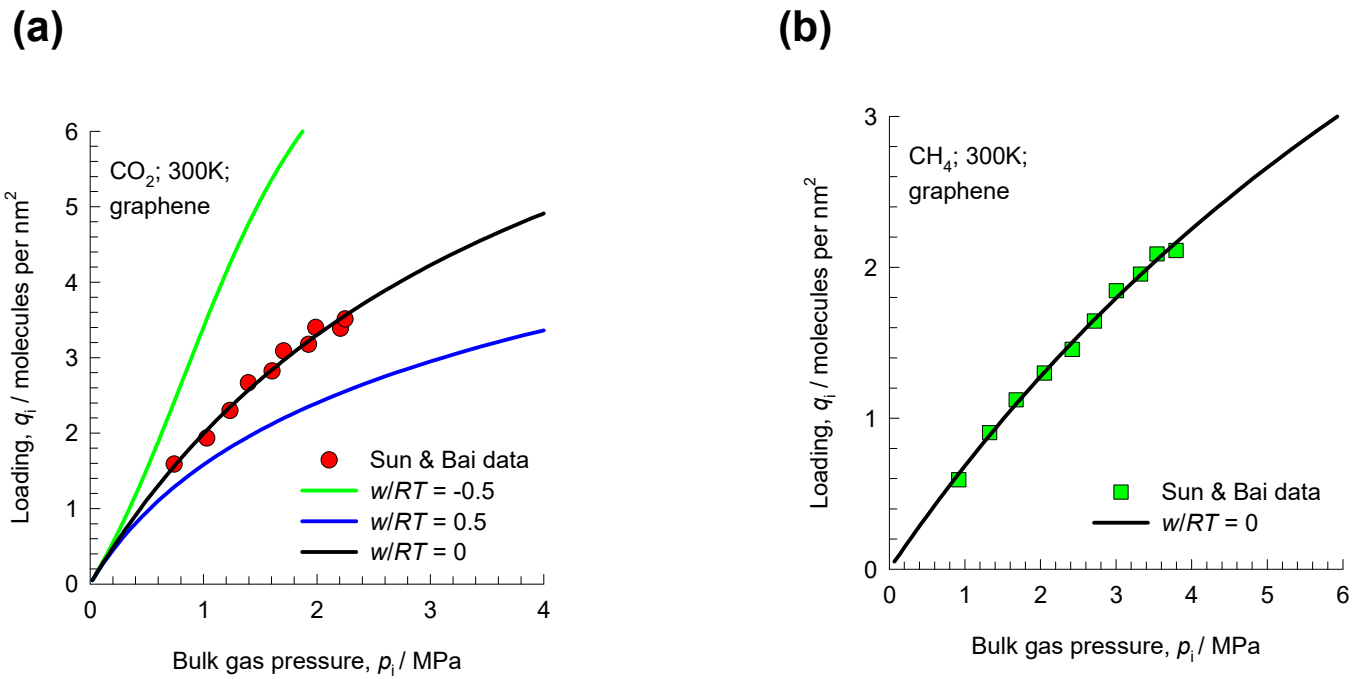

Fig. S7

Isotherm fitting to determine interaction energies

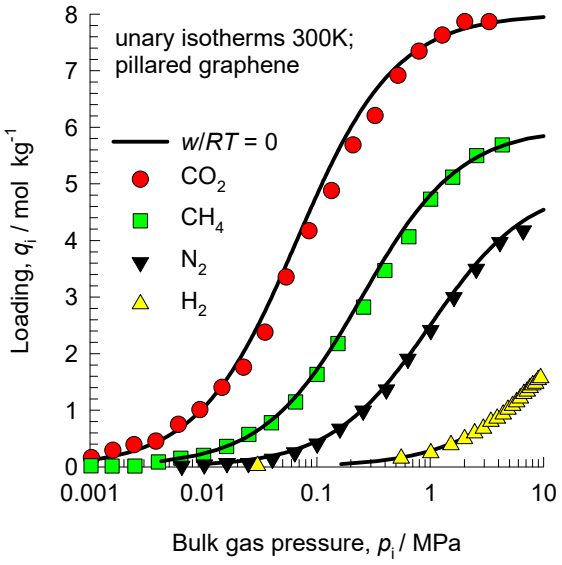

Fig. S8

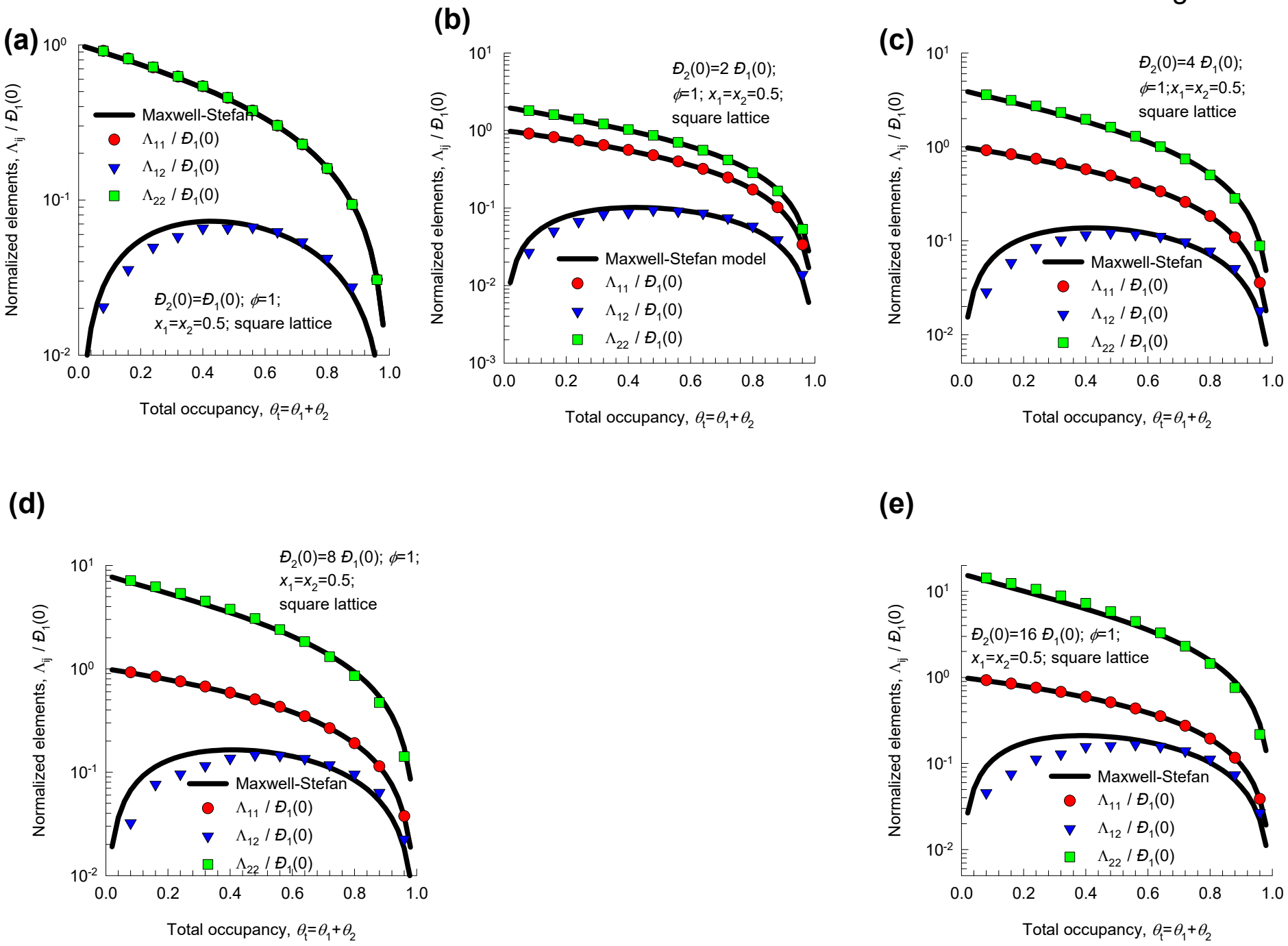
(a)
Normalized elements, Λ_{ij} / $Đ_1(0)$
Maxwell-Stefan
Λ_{11} / $Đ_1(0)$
Λ_{12} / $Đ_1(0)$
Λ_{22} / $Đ_1(0)$
$Đ_2(0)=Đ_1(0)$; ϕ=1;
$x_1=x_2$=0.5; square lattice
Total occupancy, $\theta_t=\theta_1+\theta_2$
(b)
$Đ_2(0)$=2 $Đ_1(0)$;
ϕ=1; $x_1=x_2$=0.5;
square lattice
Maxwell-Stefan model
(c)
$Đ_2(0)$=4 $Đ_1(0)$;
ϕ=1;$x_1=x_2$=0.5;
square lattice
(d)
$Đ_2(0)$=8 $Đ_1(0)$; ϕ=1;
$x_1=x_2$=0.5;
square lattice
(e)
$Đ_2(0)$=16 $Đ_1(0)$; ϕ=1;
$x_1=x_2$=0.5; square lattice

Fig. S9

(a)

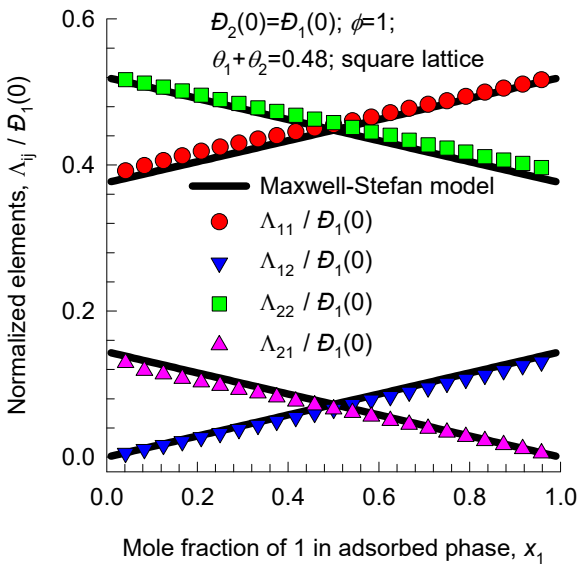
Đ2(0)=Đ1(0); ϕ=1;
θ1+θ2=0.48; square lattice
Maxwell-Stefan model
Λ11 / Đ1(0)
Λ12 / Đ1(0)
Λ22 / Đ1(0)
Λ21 / Đ1(0)
Normalized elements, Λij / Đ1(0)
Mole fraction of 1 in adsorbed phase, x1

(b)

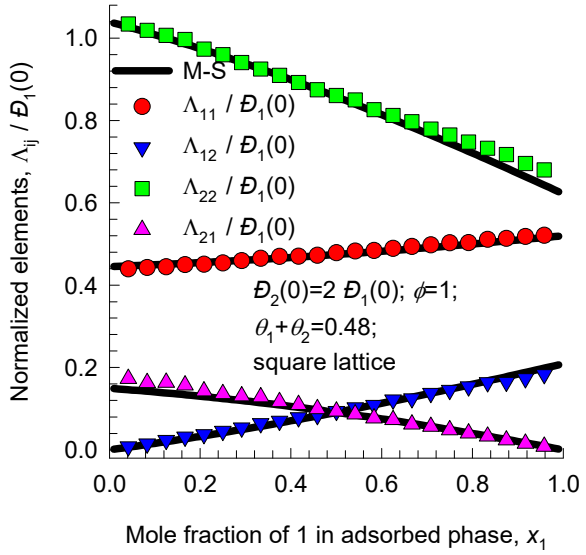
M-S
Λ11 / Đ1(0)
Λ12 / Đ1(0)
Λ22 / Đ1(0)
Λ21 / Đ1(0)
Đ2(0)=2 Đ1(0); ϕ=1;
θ1+θ2=0.48;
square lattice
Normalized elements, Λij / Đ1(0)
Mole fraction of 1 in adsorbed phase, x1

(c)

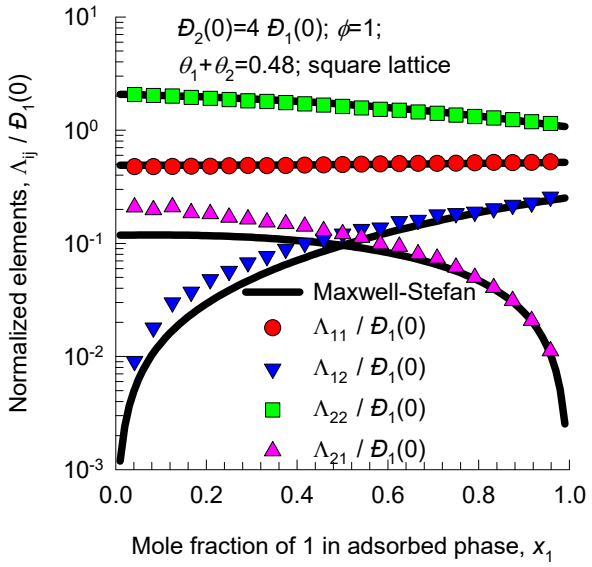
Đ2(0)=4 Đ1(0); ϕ=1;
θ1+θ2=0.48; square lattice
Maxwell-Stefan
Λ11 / Đ1(0)
Λ12 / Đ1(0)
Λ22 / Đ1(0)
Λ21 / Đ1(0)
Normalized elements, Λij / Đ1(0)
Mole fraction of 1 in adsorbed phase, x1

(d)

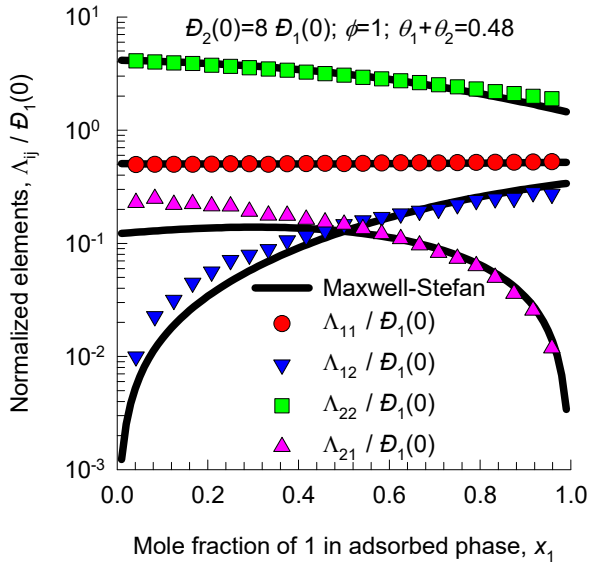
Đ2(0)=8 Đ1(0); ϕ=1; θ1+θ2=0.48
Maxwell-Stefan
Λ11 / Đ1(0)
Λ12 / Đ1(0)
Λ22 / Đ1(0)
Λ21 / Đ1(0)
Normalized elements, Λij / Đ1(0)
Mole fraction of 1 in adsorbed phase, x1

Fig. S10

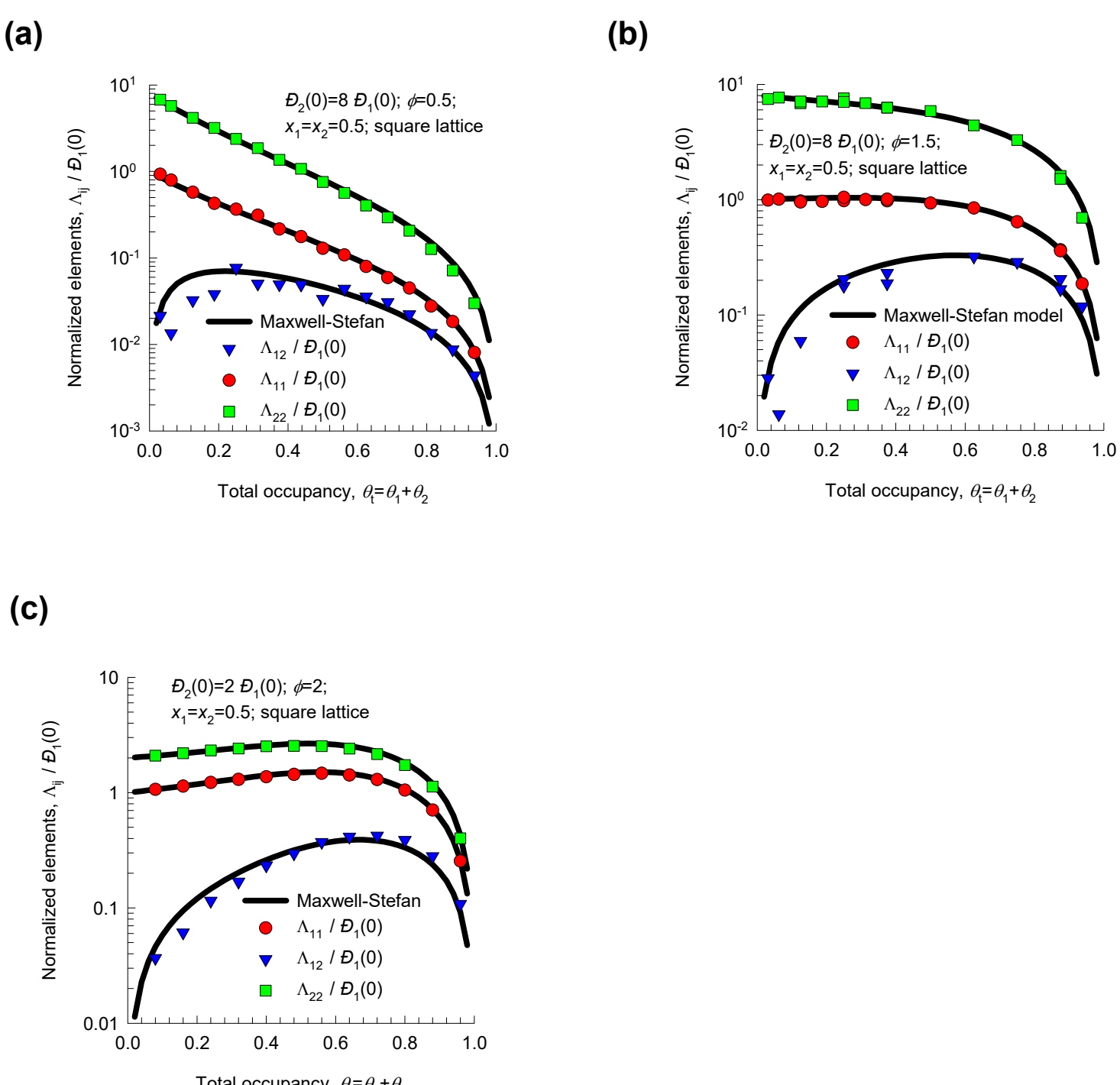
(a)
$Đ_2(0)=8\ Đ_1(0)$; $\phi=0.5$;
$x_1=x_2=0.5$; square lattice
Maxwell-Stefan
$\Lambda_{12} / Đ_1(0)$
$\Lambda_{11} / Đ_1(0)$
$\Lambda_{22} / Đ_1(0)$
Normalized elements, $\Lambda_{ij} / Đ_1(0)$
Total occupancy, $\theta_t=\theta_1+\theta_2$
(b)
$Đ_2(0)=8\ Đ_1(0)$; $\phi=1.5$;
$x_1=x_2=0.5$; square lattice
Maxwell-Stefan model
$\Lambda_{11} / Đ_1(0)$
$\Lambda_{12} / Đ_1(0)$
$\Lambda_{22} / Đ_1(0)$
Normalized elements, $\Lambda_{ij} / Đ_1(0)$
Total occupancy, $\theta_t=\theta_1+\theta_2$
(c)
$Đ_2(0)=2\ Đ_1(0)$; $\phi=2$;
$x_1=x_2=0.5$; square lattice
Maxwell-Stefan
$\Lambda_{11} / Đ_1(0)$
$\Lambda_{12} / Đ_1(0)$
$\Lambda_{22} / Đ_1(0)$
Normalized elements, $\Lambda_{ij} / Đ_1(0)$
Total occupancy, $\theta_t=\theta_1+\theta_2$

Fig. S11

(a)

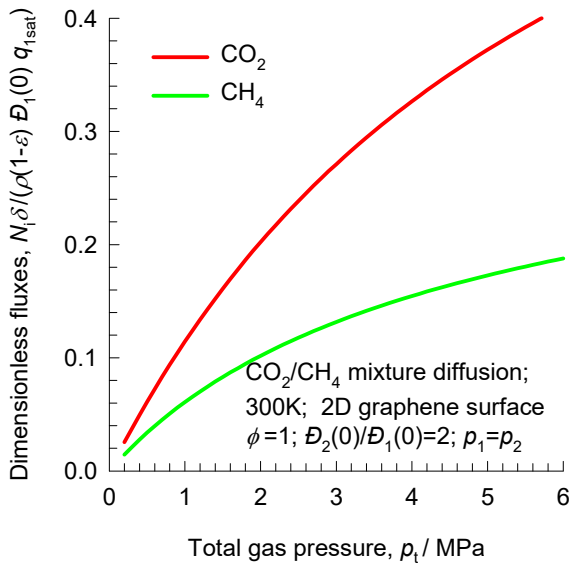
Dimensionless fluxes, $N_i\delta/(\rho(1-\varepsilon)\,Đ_1(0)\,q_{1sat})$
0.4
0.3
0.2
0.1
0.0
0
1
2
3
4
5
6
Total gas pressure, p_t / MPa
CO_2
CH_4
CO_2/CH_4 mixture diffusion;
300K; 2D graphene surface
ϕ=1; $Đ_2(0)/Đ_1(0)$=2; $p_1=p_2$

(b)

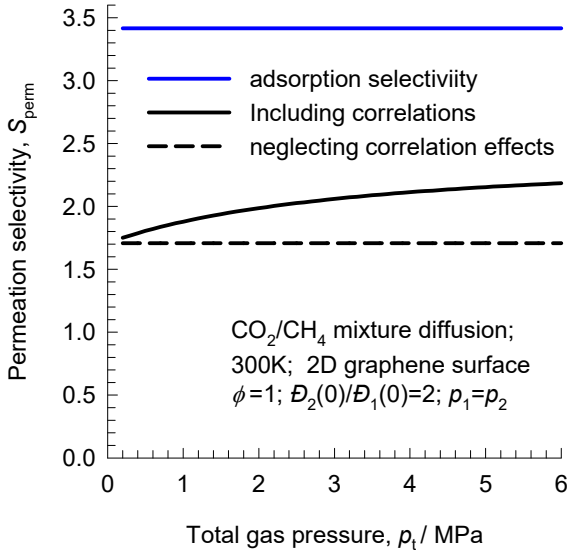
Permeation selectivity, S_{perm}
3.5
3.0
2.5
2.0
1.5
1.0
0.5
0.0
0
1
2
3
4
5
6
Total gas pressure, p_t / MPa
adsorption selectivity
Including correlations
neglecting correlation effects
CO_2/CH_4 mixture diffusion;
300K; 2D graphene surface
ϕ=1; $Đ_2(0)/Đ_1(0)$=2; $p_1=p_2$

Fig. S12

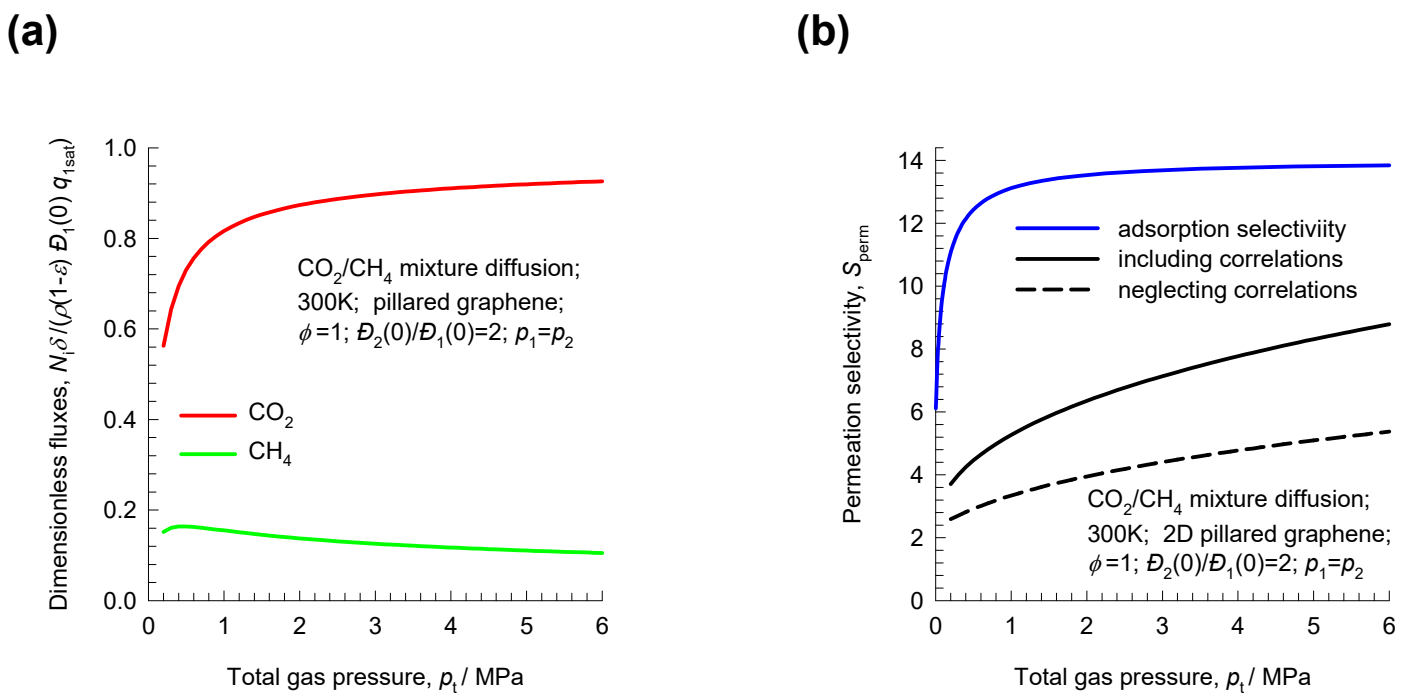
(a)
Dimensionless fluxes, $N_i\delta/(\rho(1-\varepsilon)\,Đ_1(0)\,q_{1sat})$
1.0
0.8
0.6
0.4
0.2
0.0
0
1
2
3
4
5
6
Total gas pressure, p_t / MPa
CO_2/CH_4 mixture diffusion;
300K; pillared graphene;
ϕ=1; $Đ_2(0)/Đ_1(0)$=2; $p_1=p_2$
CO_2
CH_4
(b)
Permeation selectivity, S_{perm}
14
12
10
8
6
4
2
0
0
1
2
3
4
5
6
Total gas pressure, p_t / MPa
adsorption selectiviity
including correlations
neglecting correlations
CO_2/CH_4 mixture diffusion;
300K; 2D pillared graphene;
ϕ=1; $Đ_2(0)/Đ_1(0)$=2; $p_1=p_2$

Fig. S13

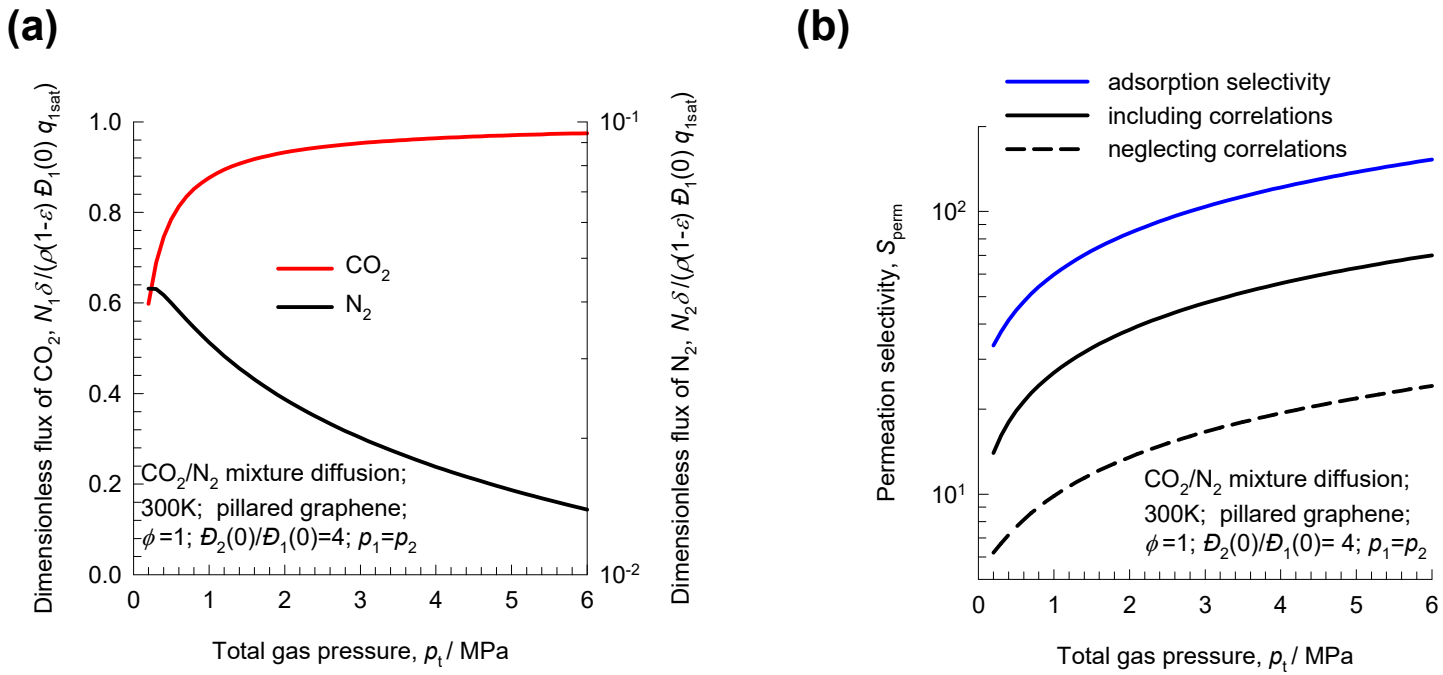
(a)
Dimensionless flux of CO2, N1δ/(ρ(1-ε) Đ1(0) q1sat)
Dimensionless flux of N2, N2δ/(ρ(1-ε) Đ1(0) q1sat)
1.0
0.8
0.6
0.4
0.2
0.0
10-1
10-2
CO2
N2
CO2/N2 mixture diffusion;
300K; pillared graphene;
ϕ=1; Đ2(0)/Đ1(0)=4; p1=p2
0
1
2
3
4
5
6
Total gas pressure, pt / MPa
(b)
adsorption selectivity
including correlations
neglecting correlations
Permeation selectivity, Sperm
102
101
CO2/N2 mixture diffusion;
300K; pillared graphene;
ϕ=1; Đ2(0)/Đ1(0)= 4; p1=p2
0
1
2
3
4
5
6
Total gas pressure, pt / MPa

Fig. S14

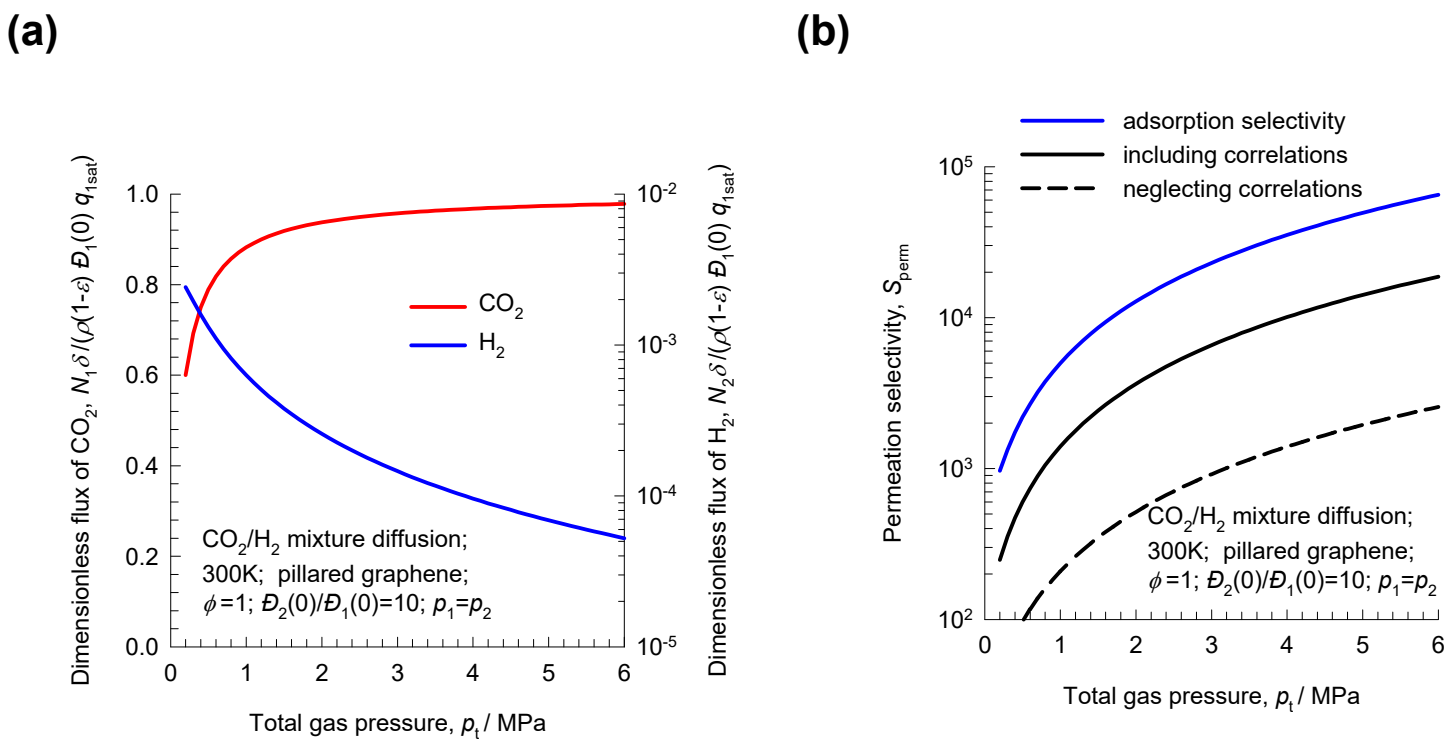
(a)
(b)
Dimensionless flux of CO2, N1δ/(ρ(1-ε) Đ1(0) q1sat)
Dimensionless flux of H2, N2δ/(ρ(1-ε) Đ1(0) q1sat)
CO2
H2
CO2/H2 mixture diffusion;
300K; pillared graphene;
ϕ=1; Đ2(0)/Đ1(0)=10; p1=p2
Total gas pressure, pt / MPa
Permeation selectivity, Sperm
adsorption selectivity
including correlations
neglecting correlations
CO2/H2 mixture diffusion;
300K; pillared graphene;
ϕ=1; Đ2(0)/Đ1(0)=10; p1=p2
Total gas pressure, pt / MPa

Fig. S15

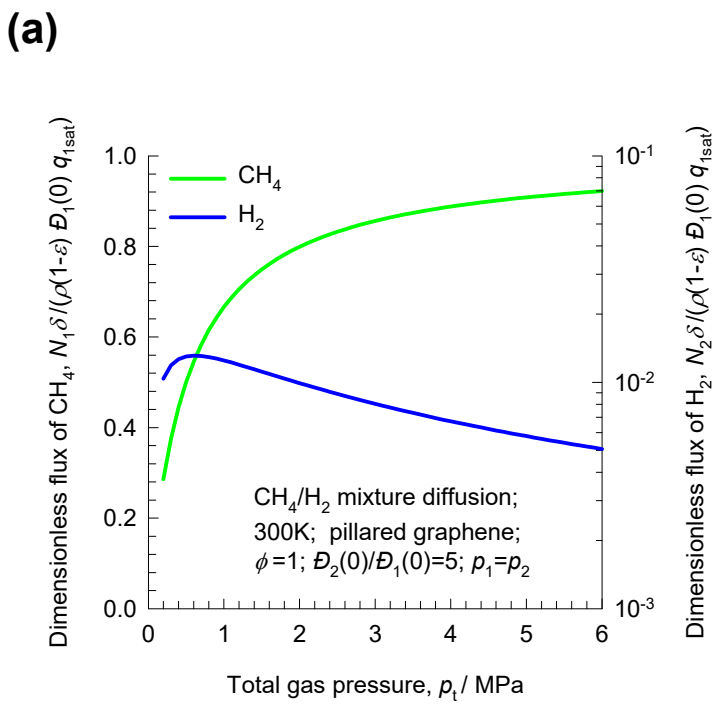
(a)
Dimensionless flux of CH4, N1δ/(ρ(1-ε) Đ1(0) q1sat)
Dimensionless flux of H2, N2δ/(ρ(1-ε) Đ1(0) q1sat)
CH4
H2
CH4/H2 mixture diffusion;
300K; pillared graphene;
ϕ=1; Đ2(0)/Đ1(0)=5; p1=p2
Total gas pressure, pt / MPa

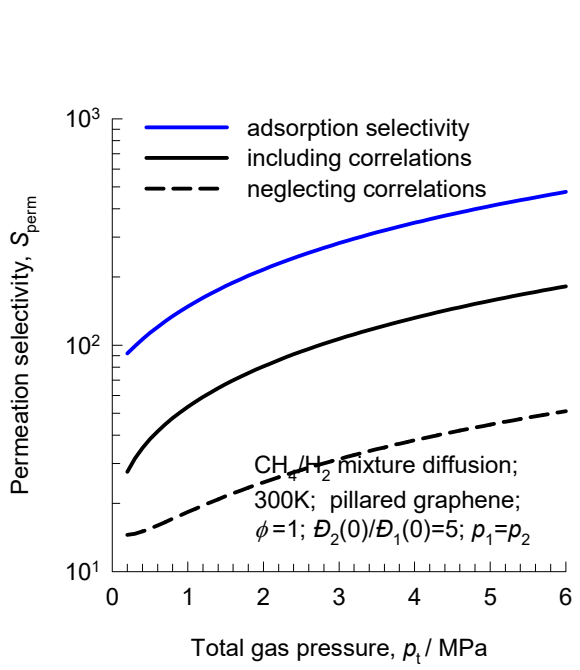
(b)
Permeation selectivity, Sperm
adsorption selectivity
including correlations
neglecting correlations
CH4/H2 mixture diffusion;
300K; pillared graphene;
ϕ=1; Đ2(0)/Đ1(0)=5; p1=p2
Total gas pressure, pt / MPa

Fig. S16

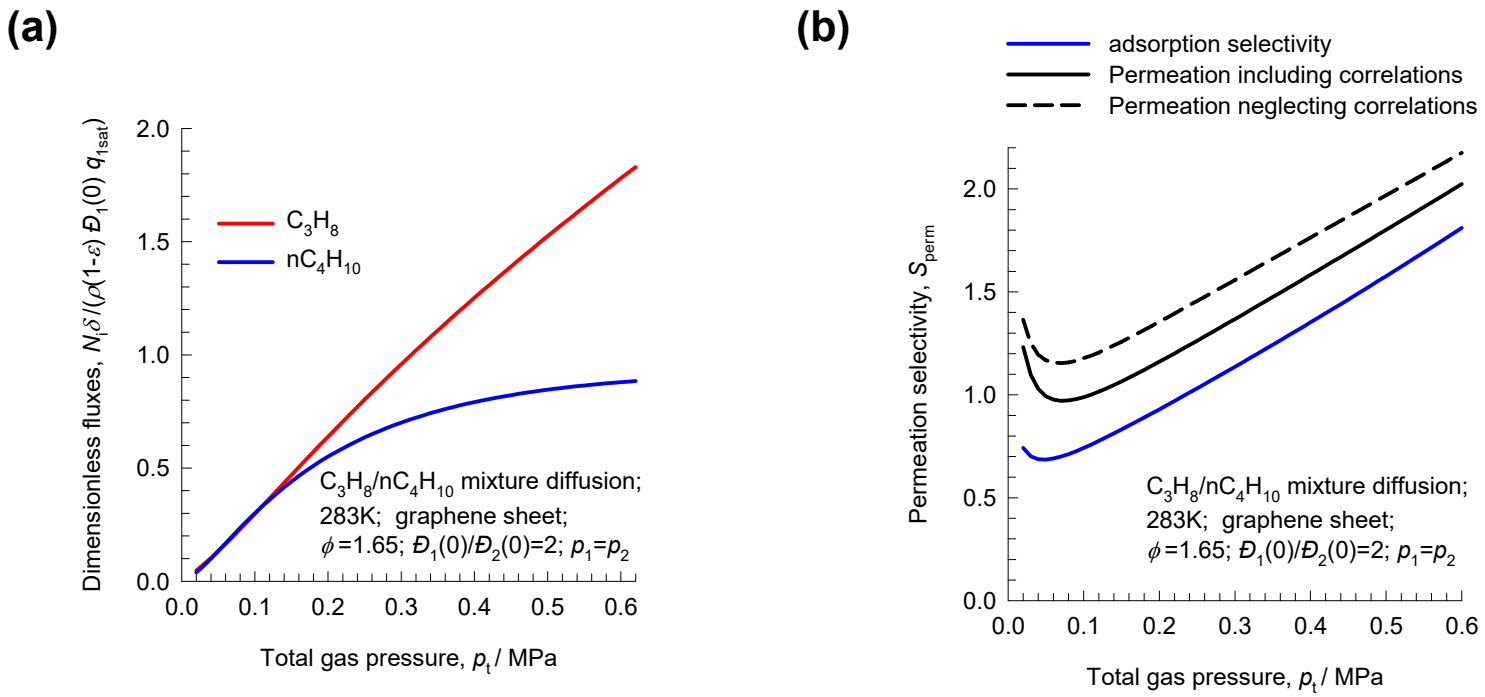
(a)
Dimensionless fluxes, $N_i\delta/(\rho(1-\varepsilon)\,Đ_1(0)\,q_{1sat})$
2.0
1.5
1.0
0.5
0.0
0.0
0.1
0.2
0.3
0.4
0.5
0.6
Total gas pressure, p_t / MPa
C_3H_8
nC_4H_{10}
C_3H_8/nC_4H_{10} mixture diffusion;
283K; graphene sheet;
ϕ=1.65; $Đ_1(0)/Đ_2(0)$=2; $p_1=p_2$
(b)
adsorption selectivity
Permeation including correlations
Permeation neglecting correlations
Permeation selectivity, S_{perm}
2.0
1.5
1.0
0.5
0.0
0.0
0.1
0.2
0.3
0.4
0.5
0.6
Total gas pressure, p_t / MPa
C_3H_8/nC_4H_{10} mixture diffusion;
283K; graphene sheet;
ϕ=1.65; $Đ_1(0)/Đ_2(0)$=2; $p_1=p_2$